

---

# A Stochastic Approximation Method for Reachability Computations

Maria Prandini<sup>1</sup> and Jianghai Hu<sup>2</sup>

<sup>1</sup> Dipartimento di Elettronica e Informazione, Politecnico di Milano, Piazza Leonardo da Vinci 32, 20133 Milano, Italy, [prandini@elet.polimi.it](mailto:prandini@elet.polimi.it)

<sup>2</sup> School of Electrical and Computer Engineering, Purdue University, West Lafayette, IN 47906, USA, [jianghai@purdue.edu](mailto:jianghai@purdue.edu)

**Summary.** We develop a grid-based method for estimating the probability that the trajectories of a given stochastic system will eventually enter a certain target set during a –possibly infinite– look-ahead time horizon. The distinguishing feature of the proposed methodology is that it rests on the approximation of the solution to stochastic differential equations by using Markov chains. From an algorithmic point of view, the probability of entering the target set is computed by appropriately propagating the transition probabilities of the Markov chain backwards in time starting from the target set during the time horizon of interest. We consider air traffic management as an application example. Specifically, we address the problem of estimating the probability that two aircraft flying in the same region of the airspace get closer than a certain safety distance and that an aircraft enters a forbidden airspace area. In this context, the target set is the set of unsafe configurations for the system, and we are estimating the probability that an unsafe situation occurs.

## 1 Introduction

In general terms, a reachability problem consists of determining if the trajectories of a given system starting from some set of initial states will eventually enter a pre-specified set.

An important application of reachability analysis is the verification of the correctness of the behavior of a system, which makes reachability analysis relevant in a variety of control applications. In particular, in many safety-critical applications a certain region of the state space is “unsafe”, and one has to verify that the system state keeps outside this unsafe set. If the outcome of safety verification is negative, then some action has to be taken to appropriately modify the system.

Given the unsafe set and the set of initial states, a safety verification problem can be reformulated as either a forward reachability problem or a backward reachability problem. Forward reachability consists in determining the set of states that a given system can reach starting from some set of

initial states. Conversely, backward reachability consists in determining the set of initial states starting from which the system will eventually enter a given target set of states. One can perform safety verification by checking either that the forward reachable set is disjoint from the unsafe set or that the backward reachable set leading to the unsafe set is disjoint from the set of initial states.

One method for safety verification is the model checking approach, which verifies safety by constructing forward/backward reachable sets based on a model of the system. The main issue of this approach is the ability to “compute” with sets, i.e., to represent sets and propagate them through the system dynamics. This process can be made fully automatic. Model checkers have in fact been developed for different classes of deterministic systems.

In the case of deterministic finite automata, sets can be represented by enumeration, and forward (backward) reachable sets can be computed starting from the given initial (target) set and adding one-step successor (predecessor) till convergence is achieved. Termination of the algorithm is guaranteed since the state space is finite. Safety verification is then “decidable” for this class of systems, that is, there does exist a computational procedure that decides in a finite number of steps whether safety is verified or not for an arbitrary deterministic finite automata. The technical challenge for the verification of deterministic finite automata is to devise algorithms and data structure to handle large state spaces.

In the case of hybrid systems, two key issues arise due to the uncountable number of states in the continuous state space: i) set representation and propagation by continuous flow is generally difficult; and ii) the state space is not finite, hence termination of the algorithm for reachable set computation is not guaranteed ([32]). Decidability results have been proven for certain classes of hybrid systems by using discrete abstraction consisting in building a finite automaton that is “equivalent” to the original hybrid system for the purpose of safety verification ([2]).

Exact methods for reachability computations exist only for a restricted class of hybrid systems with simple dynamics. In the case of more complex dynamics, approximation methods have been developed, which can be classified as “over-approximation” and “asymptotic approximation” methods.

The over-approximation methods aim at obtaining efficient over-approximations of reachable sets. The main idea is to start from sets that are easy to represent in a compact form and approximating the system dynamics so that the sets obtained through the direct or inverse evolution of the approximated system admit the same representation of the starting sets, while ensuring over-approximation of the reachable sets of the original system. Polyhedral and ellipsoidal methods ([4, 19]) belong to this category of approximation approaches.

The asymptotic approximation methods aim at obtaining an approximation of the reachable sets that converges to the true reachable sets as some accuracy parameter tends to zero. Level set methods and gridding techniques

belong to this category. In level set methods, sets are represented as the zero sublevel set of an appropriate function. The evolution of the boundary of this set through the system dynamics can be described through a Hamilton-Jacobi-Isaacs partial differential equation. An approximation to the reachable set is then obtained by a suitable numerical approximation of this equation ([26, 25]). In [30] a Markov chain approximation of a deterministic system is introduced to perform reachability analysis. The Markov chain is obtained by gridding the state space of the original system and defining the transition probabilities over the so-obtained discrete set of states so as to guarantee that admissible trajectories of the original system correspond to trajectories with non zero probability of the Markov chain. If the probability that the Markov chain enters the unsafe set is zero, then, one can conclude that the original system is safe. However, if such probability is not zero, the original system may still be safe.

In all approaches, reachability computations become more intensive as the dimension of the continuous state space grows. This is particularly critical in asymptotic approximation methods. On the other hand, the over-approximation methods have to be designed based on the characteristics of the specific system under study, and generally provide solutions to the safety verification problem that are too conservative when the system dynamics is complex and the reachable sets have arbitrary shapes. In comparison, the asymptotic approximation methods can be applied to general classes of systems and they do not require a specific shape for the reachable sets.

In many control applications, the dynamics of the system under study is subjected to the perturbation of random noises that are either inherent or present in the environment. These systems are naturally described by stochastic models, whose trajectories occur with different probabilities. For this class of systems, one can adopt either a worst-case approach or a probabilistic approach to safety verification. In the worst-case approach to safety verification, one requires all the admissible trajectories of the system to be outside the unsafe set, regardless of their probability, thus ignoring the stochastic nature of the system. In [20], for example, the system is stochastic because of some random noise signal affecting the system dynamics. However, the noise process is assumed to be bounded and is treated as if it were a deterministic signal taking values in a known compact set for the purpose of reachability computations. In the probabilistic approach to safety verification, one allows some trajectories of the system to enter the unsafe set if this event has low probability, thus avoiding the conservativeness of the worst-case approach.

A probabilistic approach to safety verification can be useful within a structured alerting system where alarms of different severity are issued depending on the level of criticality of the situation. For systems operating in a highly dynamic uncertain environment, safety has to be repeatedly verified on-line based on the updated information on the system behavior. In these applications it is then very important to have some measure of criticality for evaluating whether the selected control input is appropriate or a corrective action

should be taken to timely steer the system out of the unsafe set. A natural choice for the measure of criticality is the probability of intrusion into the unsafe set within a finite/infinite time horizon: the higher the probability of intrusion, the more critical the situation.

In this chapter, we describe a methodology for probabilistic reachability analysis of a certain class of stochastic hybrid systems governed by stochastic differential equations with time-driven jumps. The distinguishing feature of the proposed methodology is that it rests on the approximation of the solution to stochastic differential equations by using Markov chains. The basic idea is to construct a Markov chain whose state space is obtained by discretizing the original space into grids. For properly chosen transition probabilities, the Markov chain converges weakly to the solution to the stochastic differential equation as the discretization step approaches zero. Therefore, an approximation of the probability of interest can be obtained by computing the corresponding quantity for the Markov chain.

From an algorithmic point of view, we propose a backward reachability algorithm which computes for each state an estimate of the probability that the system will enter the unsafe set starting from that state by appropriately propagating the transition probabilities of the Markov chain backwards in time starting from the unsafe set during the time horizon of interest.

According to the classification of safety verification approaches mentioned above, our approach can be described as an asymptotic approximation probabilistic model checking method based on backward reachability computations.

We shall consider the problem of conflict prediction in Air Traffic Management (ATM) as an application example.

## 2 Stochastic approximation method

### 2.1 Formulation of the reachability problem

Consider an  $n$ -dimensional system whose dynamics is governed by the stochastic differential equation

$$dS(t) = a(S, t)dt + b(S)\Gamma dW(t), \quad (1)$$

during the time interval  $T = [0, t_f]$ , where 0 is the current time instant, and  $t_f$  is a positive real number (possibly infinity) representing the look-ahead time horizon. Function  $a : \mathbb{R}^n \times T \rightarrow \mathbb{R}^n$  is the drift term, function  $b : \mathbb{R}^n \rightarrow \mathbb{R}^{n \times n}$  is the diffusion term, and  $\Gamma$  is a diagonal matrix with positive entries, which modulates the variance of the standard  $n$ -dimensional Brownian motion  $W(\cdot)$ .

We suppose that  $b : \mathbb{R}^n \rightarrow \mathbb{R}^{n \times n}$  is a continuous function, whereas  $a : \mathbb{R}^n \times T \rightarrow \mathbb{R}^n$  is continuous in its first argument and only piecewise continuous in its second argument.

Let  $\mathcal{D} \subset \mathbb{R}^n$  be a set representing the unsafe region for the system.

Our objective is to evaluate the probability that  $S(t)$  enters  $\mathcal{D}$  starting from some initial state  $S(0)$  during the time interval  $T = [0, t_f]$ .

Since  $\mathcal{D}$  represents an unsafe region, which, in the ATM application introduced later, corresponds to a region where a conflict takes place, in the sequel we shall refer to the probability of interest:

$$P\{S(t) \in \mathcal{D} \text{ for some } t \in T\}, \quad (2)$$

as the *probability of conflict*.

To evaluate the probability of conflict (2) numerically, we consider an open domain  $\mathcal{U} \subset \mathbb{R}^n$  that contains  $\mathcal{D}$  and has compact support.  $\mathcal{U}$  should be large enough so that the situation can be declared safe once  $S$  ends up outside  $\mathcal{U}$ . With reference to the domain  $\mathcal{U}$ , the probability of entering the unsafe set  $\mathcal{D}$  can be expressed as

$$P_c := P\{S \text{ hits } \mathcal{D} \text{ before hitting } \mathcal{U}^c \text{ within the time interval } T\}, \quad (3)$$

where  $\mathcal{U}^c$  denotes the complement of  $\mathcal{U}$  in  $\mathbb{R}^n$ . Implicit in the above definition is that if  $S$  hits neither  $\mathcal{D}$  nor  $\mathcal{U}^c$  during  $T$ , no conflict occurs.

For the purpose of computing (3), we can assume that in equation (1),  $S$  is defined on the open domain  $\mathcal{U} \setminus \mathcal{D}$  with initial condition  $S(0)$ , and that it is stopped as soon as it hits the boundary  $\partial\mathcal{U} \cup \partial\mathcal{D}$ .

## 2.2 Markov chain approximation: weak convergence result

We now describe an approach to approximate the solution  $S(\cdot)$  to equation (1) defined on  $\mathcal{U} \setminus \mathcal{D}$  with absorption on the boundary  $\partial\mathcal{U} \cup \partial\mathcal{D}$ . The idea is to discretize  $\mathcal{U} \setminus \mathcal{D}$  into grid points that constitute the state space of a Markov chain. By carefully choosing the transition probabilities, the solution to the Markov chain will converge weakly to that of the stochastic differential equation (1) as the grid size approaches zero. Therefore, at a small grid size, a good estimate of the probability  $P_c$  in (3) is provided by the corresponding quantity associated with the Markov chain, which is much easier to compute.

To define the Markov chain, we first need to introduce some notations.

Let  $\Gamma = \text{diag}(\sigma_1, \sigma_2, \dots, \sigma_n)$ , with  $\sigma_1, \sigma_2, \dots, \sigma_n > 0$ .

Fix a grid size  $\delta > 0$ . Denote by  $\delta\mathbb{Z}^n$  the integer grids of  $\mathbb{R}^n$  scaled properly, more precisely,

$$\delta\mathbb{Z}^n = \{(m_1\eta_1\delta, m_2\eta_2\delta, \dots, m_n\eta_n\delta) \mid (m_1, m_2, \dots, m_n) \in \mathbb{Z}^n\},$$

where  $\eta_i$ ,  $i = 1, \dots, n$ , are defined as  $\eta_i := \frac{\sigma_i}{\bar{\sigma}}$ ,  $i = 1, \dots, n$ , with  $\bar{\sigma} = \max_i \sigma_i$ . For each grid point  $q \in \delta\mathbb{Z}^n$ , define the immediate neighbors set

$$\mathcal{N}_q = \{q + (i_1\eta_1\delta, i_2\eta_2\delta, \dots, i_n\eta_n\delta) \mid (i_1, i_2, \dots, i_n) \in \mathcal{I}\}, \quad (4)$$

where  $\mathcal{I} \subseteq \{0, 1, -1\}^n \setminus \{(0, 0, \dots, 0)\}$ . The immediate neighbors set  $\mathcal{N}_q$  is a subset of all the points in  $\delta\mathbb{Z}^n$  whose distance from  $q$  along the coordinate

axis  $x_i$  is at most  $\eta_i \delta$ ,  $i = 1, \dots, n$ . The larger the cardinality of  $\mathcal{N}_q$ , the more intensive the computations. For the convergence result to hold, different choices for  $\mathcal{N}_q$  are possible, which depend, in particular, on the diffusion term  $b$  in (1). For the time being, consider the immediate neighbors set as given. We shall then see possible choices for it in some specific cases.

Define  $\mathcal{Q} = (\mathcal{U} \setminus \mathcal{D}) \cap \delta\mathbb{Z}^n$ , which consists of all those grid points in  $\delta\mathbb{Z}^n$  that lie inside  $\mathcal{U}$  but outside  $\mathcal{D}$ . The interior of  $\mathcal{Q}$ , denoted by  $\mathcal{Q}^0$ , consists of all those points in  $\mathcal{Q}$  which have all their neighbors in  $\mathcal{Q}$ . The boundary of  $\mathcal{Q}$  is defined to be  $\partial\mathcal{Q} = \mathcal{Q} \setminus \mathcal{Q}^0$ , and is the union of two disjoint sets:  $\partial\mathcal{Q} = \partial\mathcal{Q}_{\mathcal{U}} \cup \partial\mathcal{Q}_{\mathcal{D}}$ , where points in  $\partial\mathcal{Q}_{\mathcal{U}}$  have at least one neighbor outside  $\mathcal{U}$ , and points in  $\partial\mathcal{Q}_{\mathcal{D}}$  have at least one neighbor inside  $\mathcal{D}$ . If a point satisfies both the conditions, then we assign it only to  $\partial\mathcal{Q}_{\mathcal{D}}$ . This will eventually lead to an overestimation of the probability of conflict. However, if  $\mathcal{U}$  is chosen to be large enough, the overestimation error is negligible.

We now define a Markov chain  $\{Q_k, k \geq 0\}$  on the state space  $\mathcal{Q}$ . Denote by  $\Delta t > 0$  the amount of time elapsing between any two successive discrete time steps  $k$  and  $k + 1$ ,  $k \geq 0$ .  $\{Q_k, k \geq 0\}$  is a time-inhomogeneous Markov chain such that:

1. each state in  $\partial\mathcal{Q}$  is an absorbing state, i.e., the state of the chain remains unchanged after it hits any of the states  $q \in \partial\mathcal{Q}$ :

$$P\{Q_{k+1} = q' | Q_k = q\} = \begin{cases} 1, & q' = q \\ 0, & \text{otherwise} \end{cases}$$

2. starting from a state  $q$  in  $\mathcal{Q}^0$ , the chain jumps to one of its neighbors in  $\mathcal{N}_q$  or stays at the same state according to transition probabilities determined by its current location  $q$  and the current time step  $k$ :

$$P\{Q_{k+1} = q' | Q_k = q\} = \begin{cases} p_{q'}^k(q), & q' \in \mathcal{N}_q \cup \{q\} \\ 0, & \text{otherwise,} \end{cases} \quad (5)$$

where  $p_{q'}^k(q)$  are functions of the drift and diffusion terms evaluated at  $q$  and time  $k\Delta t$ .

Set  $\Delta t = \lambda\delta^2$ , where  $\lambda$  is some positive constant.

Let the Markov chain be at state  $q \in \mathcal{Q}^0$  at some time step  $k$ . Define

$$\begin{aligned} m_q^k &= \frac{1}{\Delta t} E\{Q_{k+1} - Q_k | Q_k = q\}, \\ V_q^k &= \frac{1}{\Delta t} E\{(Q_{k+1} - Q_k)(Q_{k+1} - Q_k)^T | Q_k = q\}. \end{aligned}$$

Suppose that as  $\delta \rightarrow 0$ ,

$$\begin{aligned} m_q^k &\rightarrow a(s, k\Delta t), \\ V_q^k &\rightarrow b(s)\Gamma^2 b(s)^T, \end{aligned} \quad (6)$$

$\forall s \in \mathcal{U} \setminus \mathcal{D}$ , where for each  $\delta > 0$   $q$  is a point in  $\mathcal{Q}^0$  closest to  $s$ .

If the chain  $\{Q_k, k \geq 0\}$  starts from a point  $\bar{q} \in \mathcal{Q}^0$  closest to  $S(0)$ , then by Theorem 8.7.1 in [6] (see also [31]), we conclude that

**Proposition 1.** Fix  $\delta > 0$  and consider the corresponding Markov chain  $\{Q_k, k \geq 0\}$ . Denote by  $\{Q(t), t \geq 0\}$  the stochastic process that is equal to  $Q_k$  on the time interval  $[k\Delta t, (k+1)\Delta t)$  for all  $k$ , where  $\Delta t = \lambda\delta^2$ . Suppose that as  $\delta \rightarrow 0$ , the equations (6) are satisfied. Then as  $\delta \rightarrow 0$ ,  $\{Q(t), t \geq 0\}$  converges weakly to the solution  $\{S(t), t \geq 0\}$  to equation (1) defined on  $\mathcal{U} \setminus \mathcal{D}$  with absorption on the boundary  $\partial\mathcal{U} \cup \partial\mathcal{D}$ .  $\square$

*Remark 1.* As the grid size  $\delta$  decreases, the time interval between consecutive discrete time steps has to decrease for the stochastic process  $S(\cdot)$  to be approximated by a Markov chain with one-step successors limited to the immediate neighbors set. It is then not surprising that the time interval  $\Delta t$  is a decreasing function of the grid size  $\delta$  for the convergence result to hold.  $\square$

Let  $k_f := \lfloor \frac{t_f}{\Delta t} \rfloor$  be the largest integer not exceeding  $t_f/\Delta t$  ( $k_f = \infty$  if  $t_f = \infty$ ). As a result of Proposition 1, a good approximation to the probability of conflict  $P_c$  in (3) is given by

$$\begin{aligned} P_{c,\delta} &:= P\{Q_{k_f} \in \partial\mathcal{Q}_{\mathcal{D}}\} \\ &= P\{Q_k \text{ hits } \partial\mathcal{Q}_{\mathcal{D}} \text{ before hitting } \partial\mathcal{Q}_{\mathcal{U}} \text{ within } 0 \leq k \leq k_f\}, \end{aligned}$$

with the chain  $\{Q_k, k \geq 0\}$  starting from a point  $\bar{q} \in \mathcal{Q}$  closest to  $S(0)$ , for a small  $\delta$ .

### 2.3 Examples of transition probability functions

In this section, we describe a possible choice for the immediate neighbors set and the transition probabilities that is effective in guaranteeing that equations (6) (and, hence, the converge result) hold. We distinguish between two different structures of the diffusion term  $b$  that will fit the ATM application example.

#### Decoupled noise components

Suppose that the matrix  $b$  in equation (1) has the following form:  $b(s) = \beta(s)I$ , where  $\beta : \mathbb{R}^n \rightarrow \mathbb{R}$  and  $I$  is the identity matrix of size  $n$ .

Equation (1) then takes the form:

$$dS(t) = a(S, t)dt + \beta(S)\Gamma dW(t).$$

Since each component of the  $n$ -dimensional Brownian motion  $W(\cdot)$  directly affects a single component of  $S(\cdot)$ , the immediate neighbors set  $\mathcal{N}_q$ ,  $q \in \delta\mathbb{Z}^n$ , can be taken as the set of points along each one of the  $x_i$ ,  $i = 1, \dots, n$ , directions whose distance from  $q$  is  $\eta_i\delta$ ,  $i = 1, \dots, n$ , respectively. For each  $q \in \delta\mathbb{Z}^n$ ,  $\mathcal{N}_q$  is then composed of the following  $2n$  elements:

$$\begin{aligned}
q_{1+} &= q + (+\eta_1\delta, 0, \dots, 0), & q_{1-} &= q + (-\eta_1\delta, 0, \dots, 0), \\
q_{2+} &= q + (0, +\eta_2\delta, \dots, 0), & q_{2-} &= q + (0, -\eta_2\delta, \dots, 0), \\
&\vdots & &\vdots \\
q_{n+} &= q + (0, 0, \dots, +\eta_n\delta), & q_{n-} &= q + (0, 0, \dots, -\eta_n\delta),
\end{aligned}$$

Figure 1 plots the case when  $n = 3$ . Each grid point has six immediate neighbors ( $q_{1-}$ ,  $q_{1+}$ ,  $q_{2-}$ ,  $q_{2+}$ ,  $q_{3-}$ , and  $q_{3+}$ ): two ( $q_{1-}$  and  $q_{1+}$ ) at a distance  $\eta_1\delta$  along direction  $x_1$ , two ( $q_{2-}$  and  $q_{2+}$ ) at a distance  $\eta_2\delta$  along direction  $x_2$ , and two ( $q_{3-}$  and  $q_{3+}$ ) at a distance  $\eta_3\delta$  along direction  $x_3$ .

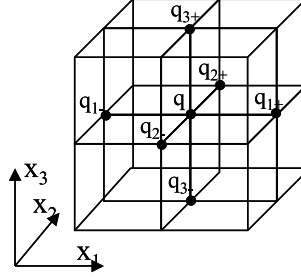


**Fig. 1.** Neighboring grid points in the three dimensional case.

We now define the transition probabilities in (5):  
If  $q \in \mathcal{Q}^0$ , then

$$\begin{aligned}
P\{Q_{k+1} = q' \mid Q_k = q\} &= \\
&\begin{cases} p_q^k(q) = \frac{\xi_0^k(q)}{C_q^k}, & q' = q \\ p_{q_{i+}}^k(q) = \frac{\exp(\delta\xi_i^k(q))}{C_q^k}, & q' = q_{i+}, i = 1, \dots, n \\ p_{q_{i-}}^k(q) = \frac{\exp(-\delta\xi_i^k(q))}{C_q^k}, & q' = q_{i-}, i = 1, \dots, n \\ 0, & \text{otherwise,} \end{cases} \quad (7)
\end{aligned}$$

where

$$\xi_0^k(q) = \frac{2}{\lambda\sigma^2\beta(q)^2} - 2n \quad \xi_i^k(q) = \frac{[a(q, k\Delta t)]_i}{\eta_i\sigma^2\beta(q)^2}, \quad i = 1, \dots, n$$

$$C_q^k = 2 \sum_{i=1}^n \cosh(\delta\xi_i^k(q)) + \xi_0^k(q).$$

$\lambda$  is a positive constant that has to be chosen small enough such that  $\xi_0^k(q)$  defined above is positive for all  $q \in \mathcal{Q}$  and all  $k \geq 0$ . In particular, this is guaranteed if

$$0 < \lambda \leq (n\sigma_1^2 \max_{s \in \mathcal{U} \setminus \mathcal{D}} \beta(s)^2)^{-1}. \quad (8)$$

As for  $\Delta t$ , we set  $\Delta t = \lambda \delta^2$ .

A direct computation shows that, with this choice for the neighboring set, the transition probabilities, and  $\Delta t$ , for each  $q \in \mathcal{Q}^0$  and  $k \geq 0$

$$m_q^k = \frac{2}{\lambda \delta C_q^k} \begin{bmatrix} \eta_1 \text{sh}(\delta \xi_1^k(q)) \\ \eta_2 \text{sh}(\delta \xi_2^k(q)) \\ \vdots \\ \eta_n \text{sh}(\delta \xi_n^k(q)) \end{bmatrix},$$

$$V_q^k = \frac{2}{\lambda C_q^k} \text{diag}(\eta_1^2 \text{csh}(\delta \xi_1^k(q)), \eta_2^2 \text{csh}(\delta \xi_2^k(q)), \dots, \eta_n^2 \text{csh}(\delta \xi_n^k(q))).$$

It is then easily verified that the equations in (6) are satisfied, which in turn leads to the weak convergence result in Proposition 1.

### Coupled noise components

We consider the case when the dimension  $n$  of  $S$  is even and matrix  $\Gamma = \text{diag}(\sigma_1, \sigma_2, \dots, \sigma_n)$  satisfies  $\sigma_h = \sigma_{h+n/2} > 0$ ,  $h = 1, \dots, n/2$ . Moreover, we assume that the diffusion term  $b$  in equation (1) takes the following form

$$b(s) = \begin{bmatrix} I & \alpha(s)I \\ \alpha(s)I & I \end{bmatrix}^{1/2}$$

with  $\alpha : \mathbb{R}^n \rightarrow [0, 1]$ . The components  $h$  and  $h + n/2$  of  $S(\cdot)$  are then both directly affected only by the components  $h$  and  $h + n/2$  of  $W(\cdot)$ , for every  $h = 1, 2, \dots, n/2$ . Based on this observation, the immediate neighbors set  $\mathcal{N}_q$ ,  $q \in \delta \mathbb{Z}^n$ , can be chosen as follows:

$$\mathcal{N}_q = \{q + (i_1 \eta_1 \delta, i_2 \eta_2 \delta, \dots, i_n \eta_n \delta) \mid (i_1, i_2, \dots, i_n) \in \mathcal{I}\},$$

where  $\mathcal{I} = \{(i_1, i_2, \dots, i_n) \mid \exists h \text{ such that } i_h = \pm 1, i_{h+n/2} = \pm 1, i_j = 0, \forall j \neq h, h + n/2\}$ . The  $2n$  elements of  $\mathcal{N}_q$  have the following expression

$$\begin{aligned} q_{1++} &= q + (+\eta_1 \delta, 0, \dots, 0, +\eta_1 \delta, 0, \dots, 0) \\ q_{1--} &= q + (-\eta_1 \delta, 0, \dots, 0, -\eta_1 \delta, 0, \dots, 0) \\ q_{1+-} &= q + (+\eta_1 \delta, 0, \dots, 0, -\eta_1 \delta, 0, \dots, 0) \\ q_{1-+} &= q + (-\eta_1 \delta, 0, \dots, 0, +\eta_1 \delta, 0, \dots, 0) \\ q_{2++} &= q + (0, +\eta_2 \delta, \dots, 0, 0, +\eta_2 \delta, \dots, 0) \\ q_{2--} &= q + (0, -\eta_2 \delta, \dots, 0, 0, -\eta_2 \delta, \dots, 0) \\ q_{2+-} &= q + (0, +\eta_2 \delta, \dots, 0, 0, -\eta_2 \delta, \dots, 0) \\ q_{2-+} &= q + (0, -\eta_2 \delta, \dots, 0, 0, +\eta_2 \delta, \dots, 0) \\ &\vdots \\ q_{(n/2)++} &= q + (0, 0, \dots, 0, +\eta_{n/2} \delta, \dots, 0, 0, \dots, 0, +\eta_{n/2} \delta) \\ q_{(n/2)--} &= q + (0, 0, \dots, 0, -\eta_{n/2} \delta, \dots, 0, 0, \dots, 0, -\eta_{n/2} \delta) \\ q_{(n/2)+-} &= q + (0, 0, \dots, 0, +\eta_{n/2} \delta, \dots, 0, 0, \dots, 0, -\eta_{n/2} \delta) \\ q_{(n/2)-+} &= q + (0, 0, \dots, 0, -\eta_{n/2} \delta, \dots, 0, 0, \dots, 0, +\eta_{n/2} \delta), \end{aligned}$$

where we used the fact that  $\eta_i = \frac{\sigma_i}{\sigma} = \frac{\sigma_{i+n/2}}{\sigma} = \eta_{i+n/2}$ ,  $i = 1, \dots, n/2$ .

We now define the transition probabilities in (5):

If  $q \in \mathcal{Q}^0$ , then

$$P\{Q_{k+1} = q' | Q_k = q\} = \begin{cases} p_q^k(q) = \frac{\xi_0^k(q)}{C}, & q' = q \\ p_{q_{i++}}^k(q) = \frac{(1 + \alpha(q)) \exp(\delta \xi_{i++}^k(q))}{C \operatorname{csh}(\delta \xi_{i++}^k(q))}, & q' = q_{i++}, i = 1, \dots, n/2 \\ p_{q_{i--}}^k(q) = \frac{(1 + \alpha(q)) \exp(-\delta \xi_{i++}^k(q))}{C \operatorname{csh}(\delta \xi_{i++}^k(q))}, & q' = q_{i--}, i = 1, \dots, n/2 \\ p_{q_{i+-}}^k(q) = \frac{(1 - \alpha(q)) \exp(\delta \xi_{i+-}^k(q))}{C \operatorname{csh}(\delta \xi_{i+-}^k(q))}, & q' = q_{i+-}, i = 1, \dots, n/2 \\ p_{q_{i-+}}^k(q) = \frac{(1 - \alpha(q)) \exp(-\delta \xi_{i+-}^k(q))}{C \operatorname{csh}(\delta \xi_{i+-}^k(q))}, & q' = q_{i-+}, i = 1, \dots, n/2 \\ 0, & \text{otherwise,} \end{cases} \quad (9)$$

where

$$\begin{aligned} \xi_0^k(q) &= \frac{4}{\lambda \bar{\sigma}^2} - 2n, \\ \xi_{i++}^k(q) &= \frac{[a(q, k \Delta t)]_i + [a(q, k \Delta t)]_{i+n/2}}{\eta_i \bar{\sigma}^2 (1 + \alpha(q))}, \quad i = 1, \dots, n/2 \\ \xi_{i+-}^k(q) &= \frac{[a(q, k \Delta t)]_i - [a(q, k \Delta t)]_{i+n/2}}{\eta_i \bar{\sigma}^2 (1 - \alpha(q))}, \quad i = 1, \dots, n/2 \\ C &= \frac{4}{\lambda \bar{\sigma}^2}, \end{aligned}$$

$\lambda$  is a positive constant that has to be chosen small enough such that  $\xi_0^k(q)$  defined above is positive for all  $q \in \mathcal{Q}$  and all  $k \geq 0$ . In particular, this is guaranteed if

$$0 < \lambda \leq (\bar{\sigma}^2 n/2)^{-1}. \quad (10)$$

The time elapsed between successive jumps is set equal to  $\Delta t = \lambda \bar{\sigma}^2$ .

It can be verified that, with this choice for the neighboring set, the transition probabilities, and  $\Delta t$ , for each  $q \in \mathcal{Q}^0$  and each  $k \geq 0$ ,

$$m_q^k = \frac{2}{\lambda \delta C} \begin{bmatrix} \eta_1(1 + \alpha(q)) \frac{\text{sh}(\delta \xi_{1++}^k(q))}{\text{csh}(\delta \xi_{1++}^k(q))} + \eta_1(1 - \alpha(q)) \frac{\text{sh}(\delta \xi_{1+-}^k(q))}{\text{csh}(\delta \xi_{1+-}^k(q))} \\ \vdots \\ \eta_{n/2}(1 + \alpha(q)) \frac{\text{sh}(\delta \xi_{(n/2)++}^k(q))}{\text{csh}(\delta \xi_{(n/2)++}^k(q))} + \eta_{n/2}(1 - \alpha(q)) \frac{\text{sh}(\delta \xi_{(n/2)+-}^k(q))}{\text{csh}(\delta \xi_{(n/2)+-}^k(q))} \\ \eta_1(1 + \alpha(q)) \frac{\text{sh}(\delta \xi_{1++}^k(q))}{\text{csh}(\delta \xi_{1++}^k(q))} - \eta_1(1 - \alpha(q)) \frac{\text{sh}(\delta \xi_{1+-}^k(q))}{\text{csh}(\delta \xi_{1+-}^k(q))} \\ \vdots \\ \eta_{n/2}(1 + \alpha(q)) \frac{\text{sh}(\delta \xi_{(n/2)++}^k(q))}{\text{csh}(\delta \xi_{(n/2)++}^k(q))} - \eta_{n/2}(1 - \alpha(q)) \frac{\text{sh}(\delta \xi_{(n/2)+-}^k(q))}{\text{csh}(\delta \xi_{(n/2)+-}^k(q))} \end{bmatrix},$$

$$V_q^k = \begin{bmatrix} I & \alpha(q)I \\ \alpha(q)I & I \end{bmatrix} \Gamma^2$$

So if  $\delta \rightarrow 0$  and we always choose  $q$  to be a point in  $\mathcal{Q}^0$  closest to a fixed  $s \in \mathcal{U} \setminus \mathcal{D}$ , then

$$\begin{aligned} m_q^k &\rightarrow a(s, k\Delta t) \\ V_q^k &\rightarrow \begin{bmatrix} I & \alpha(q)I \\ \alpha(q)I & I \end{bmatrix} \Gamma^2 = b(s)\Gamma^2 b(s)^T. \end{aligned}$$

Therefore, we conclude that Proposition 1 holds in this case as well.

#### 2.4 An iterative algorithm for reachability computations

We next describe an iterative procedure to compute the probability  $P_{c,\delta}$  that approximates the probability of conflict  $P_c$  in (3):

$$\begin{aligned} P_{c,\delta} &:= P\{Q_{k_f} \in \partial\mathcal{Q}_D\} \\ &= P\{Q_k \text{ hits } \partial\mathcal{Q}_D \text{ before hitting } \partial\mathcal{Q}_U \text{ within } 0 \leq k \leq k_f\}, \end{aligned}$$

with the chain  $\{Q_k, k \geq 0\}$  starting from a point  $\bar{q} \in \mathcal{Q}$  closest to  $S(0)$ .

We address both the finite and infinite horizon cases ( $k_f < \infty$  and  $k_f = \infty$ ).

Let

$$P_{c,\delta}^{(k)}(q) := P\{Q_{k_f} \in \partial\mathcal{Q}_D \mid Q_k = q\}, \quad (11)$$

be a set of functions defined on  $\mathcal{Q}$  and indexed by  $k = 0, 1, \dots, k_f$ . Since the chain  $\{Q_k, k \geq 0\}$  starts at  $\bar{q}$  at  $k = 0$ , the desired quantity  $P_{c,\delta}$  can be expressed in terms of the introduced functions as  $P_{c,\delta}^{(0)}(\bar{q})$ . The procedures described below determine the whole set of functions  $P_{c,\delta}^{(k)} : \mathcal{Q} \rightarrow \mathbb{R}$  for  $k =$

$0, 1, \dots, k_f$ . This has the advantage that at any future time  $t \in [0, t_f]$  an estimate of the probability of conflict over the new time horizon  $[t, t_f]$  is readily available, eliminating the need for re-computation. As a matter of fact, for each  $t \in [0, t_f]$ ,  $P_{c,\delta}^{(\lfloor t/\Delta t \rfloor)} : \mathcal{Q} \rightarrow \mathbb{R}$  represents an estimate of the probability of conflict over the time horizon  $[t, t_f]$  as a function of the value taken by the state at time  $t$ .

To compute  $P_{c,\delta}^{(0)}$ , fix a  $k$  such that  $0 \leq k < k_f$ . It is easily seen then that  $P_{c,\delta}^{(k)} : \mathcal{Q} \rightarrow \mathbb{R}$  satisfies the following recursive equation

$$P_{c,\delta}^{(k)}(q) = \begin{cases} p_q^k(q)P_{c,\delta}^{(k+1)}(q) + \sum_{q' \in \mathcal{N}_q} p_{q'}^k(q)P_{c,\delta}^{(k+1)}(q'), & q \in \mathcal{Q}^0 \\ 1, & q \in \partial\mathcal{Q}_D \\ 0, & q \in \partial\mathcal{Q}_U. \end{cases} \quad (12)$$

This is the key equation to compute  $P_{c,\delta}^{(0)}$ .

### Finite horizon

In the finite horizon case ( $k_f < \infty$ ), the probability  $P_{c,\delta} = P_{c,\delta}^{(0)}(\bar{q})$  can be computed by iterating equation (12) backward  $k_f$  times starting from  $k = k_f - 1$  and using the initialization  $P_{c,\delta}^{(k_f)}(q) = \bar{P}(q)$ ,  $q \in S$ , where

$$\bar{P}(q) = \begin{cases} 1, & \text{if } q \in \partial S_D \\ 0, & \text{otherwise.} \end{cases} \quad (13)$$

The reason for the above initialization is obvious considering the definition (11) of  $P_{c,\delta}^{(k)}$ .

The procedure to compute an approximation of  $P_c$  in the finite horizon case is summarized in the following algorithm.

**Algorithm 1** Given  $S(0)$ ,  $a : \mathbb{R}^n \times T \rightarrow \mathbb{R}^n$ ,  $b : \mathbb{R}^n \rightarrow \mathbb{R}^{n \times n}$ ,  $\Gamma$ , and  $\mathcal{D}$ , then

1. Select the open set  $\mathcal{U} \subset \mathbb{R}^n$  containing  $\mathcal{D}$ , and fix  $\delta > 0$ .
2. Define the Markov chain  $\{Q_k, k \geq 0\}$  with state space  $\mathcal{Q} = (\mathcal{U} \setminus \mathcal{D}) \cap \delta\mathbb{Z}^n$  and appropriate transition probabilities.
3. Set  $\bar{k} = k_f$  and initialize  $P_{c,\delta}^{(\bar{k})}$  with  $\bar{P}$  defined in equation (13).
4. For  $k = \bar{k} - 1, \dots, 0$ , compute  $P_{c,\delta}^{(k)}$  from  $P_{c,\delta}^{(k+1)}$  according to equation (12).
5. Choose a point  $\bar{q}$  in  $S$  closest to  $S(0)$  and set  $P_{c,\delta} = P_{c,\delta}^{(0)}(\bar{q})$ .

As for the choice of the grid size  $\delta$ , one has to take into consideration different aspects:

- i) In a time interval of length  $\Delta t$ , the maximal distance that the Markov chain can travel is  $\eta_i \delta$  along the direction  $x_i$ ,  $i = 1, \dots, n$ . Thus given  $\mathcal{U}$ ,

for the diffusion process  $S(t)$  to be approximated by the Markov chain, the component along the  $x_i$  axis  $|[a(\cdot, \cdot)]_i|$  of  $a(\cdot, \cdot)$  has to be upper bounded roughly by  $\frac{\eta_i \delta}{\Delta t}$  over  $\mathcal{U} \setminus \mathcal{D} \times T$ , for any  $i = 1, \dots, n$ . In view of Remark 1, this condition translates into upper bounds on the admissible values for  $\delta$ . In particular, in the aircraft safety analysis case  $\Delta t = \lambda \delta^2$ , hence  $\delta \leq \min_i \frac{\eta_i}{\lambda | [a(\cdot, \cdot)]_i |}$ . Thus, fast diffusion processes cannot be simulated by Markov chains corresponding to large  $\delta$ 's.

- ii) For a fixed grid size  $\delta$ , the size of the state space  $\mathcal{Q}$  is of the order of  $1/\delta^n$ , so each iteration in Algorithm 1 takes a time proportional to  $1/\delta^n$ . The number of iterations is given by  $k_f \simeq t_f/\Delta t$ . If  $\Delta t$  is proportional to  $\delta^2$  as in the safety analysis case, the running time of Algorithm 1 is proportional to  $1/\delta^{n+2}$ .

Therefore, for small  $\delta$ 's the running time may be too long, but large  $\delta$ 's may not allow for the simulation of fast moving processes. A suitable  $\delta$  is a compromise between these two conflicting requirements.

### Infinite horizon

In the infinite horizon case  $k_f = \infty$ , hence Algorithm 1 cannot be applied directly since it would take infinitely many iterations. In this section we consider a special case in which this difficulty can be easily overcome.

We start by rewriting the iteration law (12) in matrix form. Arrange the sequence  $\{P_{c,\delta}^{(k)}(q), q \in \mathcal{Q}^0\}$  into a long column vector according to some fixed ordering of the points in  $\mathcal{Q}^0$ , and denote it by  $\mathbf{P}_{c,\delta}^{(k)} \in \mathbb{R}^{|\mathcal{Q}^0|}$ . Here  $|\mathcal{Q}^0|$  is the cardinality of  $\mathcal{Q}^0$ . Then equation (12) can be written as

$$\mathbf{P}_{c,\delta}^{(k)} = \mathbf{A}^{(k)} \mathbf{P}_{c,\delta}^{(k+1)} + \mathbf{b}^{(k)} \quad (14)$$

for suitably chosen matrix  $\mathbf{A}^{(k)} \in \mathbb{R}^{|\mathcal{Q}^0| \times |\mathcal{Q}^0|}$  and vector  $\mathbf{b}^{(k)} \in \mathbb{R}^{|\mathcal{Q}^0|}$ . Note that  $\mathbf{A}^{(k)}$  is a sparse positive matrix with the property that the sum of its elements on each row is smaller than or equal to 1, where equality holds if and only if that row corresponds to a point in  $(\mathcal{Q}^0)^0$ , the interior of  $\mathcal{Q}^0$  consisting of all those points in  $\mathcal{Q}^0$  whose immediate neighbors all belong to  $\mathcal{Q}^0$ . On the other hand,  $\mathbf{b}^{(k)}$  is a positive vector with nonzero elements on exactly those rows corresponding to points on the boundary  $\partial(\mathcal{Q}^0) = \mathcal{Q}^0 \setminus (\mathcal{Q}^0)^0$  of  $\mathcal{Q}^0$ . Both  $\mathbf{A}^{(k)}$  and  $\mathbf{b}^{(k)}$  depend on the grid size  $\delta$ . We do not write it explicitly to simplify the notation.

Suppose that from some time instant  $t_c$  on,  $a(s, t)$ ,  $s \in \mathbb{R}^n$ ,  $t \in T$ , remain constant in time. Under this assumption, we have that  $\mathbf{A}^{(k)} \equiv \mathbf{A}$  and  $\mathbf{b}^{(k)} \equiv \mathbf{b}$  for  $k > k_c := \lfloor \frac{t_c}{\Delta t} \rfloor$ . Hence, for  $k > k_c$  equation (14) becomes

$$\mathbf{P}_{c,\delta}^{(k)} = \mathbf{A} \mathbf{P}_{c,\delta}^{(k+1)} + \mathbf{b}. \quad (15)$$

We next address the problem of computing  $\mathbf{P}_{c,\delta}^{(k_c+1)}$ . Once we have determined  $\mathbf{P}_{c,\delta}^{(k_c+1)}$ , we can execute Algorithm 1 with step 2 replaced by

2'. Set  $\bar{k} = k_c + 1$  and initialize  $P_{c,\delta}^{(\bar{k})}$  with  $P_{c,\delta}^{(k_c+1)}$ .

to determine the approximation  $P_{c,\delta}^{(0)}(\bar{q})$  of  $P_c$ .

The procedure to compute  $\mathbf{P}_{c,\delta}^{(k_c+1)}$  rests on the following lemma.

**Lemma 1.** *The eigenvalues of  $\mathbf{A}$  are all in the interior of the unit disk of the complex plane.  $\square$*

*Proof.* Suppose that  $\mathbf{A}$  has an eigenvalue  $\gamma$  with  $|\gamma| \geq 1$ , and let  $\mathbf{v}$  be an eigenvector such that  $\mathbf{A}\mathbf{v} = \gamma\mathbf{v}$ . Assume that  $|\mathbf{v}_i| = \max(|\mathbf{v}_1|, \dots, |\mathbf{v}_{|\mathcal{Q}^0|}|)$  for some  $i$ . Then

$$|\mathbf{v}_i| \leq |\gamma\mathbf{v}_i| = |[\mathbf{A}\mathbf{v}]_i| \leq \sum_{j=1}^{|\mathcal{Q}^0|} \mathbf{A}_{ij}|\mathbf{v}_j| \leq \sum_{j=1}^{|\mathcal{Q}^0|} \mathbf{A}_{ij}|\mathbf{v}_i| \leq |\mathbf{v}_i|,$$

which is possible only if  $|\mathbf{v}_1| = \dots = |\mathbf{v}_{|\mathcal{Q}^0|}|$ . However, this leads to a contradiction since by changing  $i$  in the above equation to one such that  $\sum_{j=1}^{|\mathcal{Q}^0|} \mathbf{A}_{ij} < 1$ , one gets  $|\mathbf{v}_i| < |\mathbf{v}_i|$ .  $\square$

Based on Lemma 1, we draw the following facts regarding equation (15):

**Lemma 2.** *Consider equation*

$$\mathbf{P}^{(k)} = \mathbf{A}\mathbf{P}^{(k+1)} + \mathbf{b}. \quad (16)$$

*i) There is a unique  $\mathbf{P} \in \mathbb{R}^{|\mathcal{Q}^0|}$  satisfying*

$$\mathbf{P} = \mathbf{A}\mathbf{P} + \mathbf{b}. \quad (17)$$

*ii) Starting from any initial value  $\mathbf{P}^{(k_0)}$  at some  $k_0$  and iterating equation (16) backward in time,  $\mathbf{P}^{(k)}$  converges to the fix point  $\mathbf{P}$  as  $k \rightarrow -\infty$ . Moreover, if  $\mathbf{P}^{(k_0)} \geq \mathbf{P}$ , then  $\mathbf{P}^{(k)} \geq \mathbf{P}$  for all  $k \leq k_0$ . Conversely, if  $\mathbf{P}^{(k_0)} \leq \mathbf{P}$ , then  $\mathbf{P}^{(k)} \leq \mathbf{P}$  for all  $k \leq k_0$ . Note that here the symbols  $\geq$  and  $\leq$  denote component-wise comparison between vectors.  $\square$*

*Proof.*  $\mathbf{P} = (I - \mathbf{A})^{-1}\mathbf{b}$  since  $I - \mathbf{A}$  is invertible by Lemma 1. Define  $\mathbf{e}^{(k)} = \mathbf{P}^{(k)} - \mathbf{P}$ . Then  $\mathbf{e}^{(k)} = \mathbf{A}\mathbf{e}^{(k+1)}$ . So by Lemma 1,  $\mathbf{e}^{(k)}$  converges to 0 as  $k \rightarrow -\infty$ . The last conclusion is a direct consequence of the fact that all components of the matrix  $\mathbf{A}$  and vector  $\mathbf{b}$  are nonnegative.  $\square$

Lemma 2 shows that equation (15) admits a fixed point  $\mathbf{P}$  to which  $\mathbf{P}^{(k)}$  obtained by iterating from any initial condition converges as  $k \rightarrow -\infty$ . Such a fixed point is in fact the desired quantity  $\mathbf{P}_{c,\delta}^{(k_c+1)}$ . Thus one way of computing  $\mathbf{P}_{c,\delta}^{(k_c+1)}$  is to solve the linear equation  $(I - \mathbf{A})\mathbf{P}_{c,\delta}^{(k_c+1)} = \mathbf{b}$  directly, using sparse matrix computation tools if possible. In our simulations, we determined  $\mathbf{P}_{c,\delta}^{(k_c+1)}$  by iterating equation (16) starting at some  $k_0$  from two initial conditions  $\mathbf{P}_l^{(k_0)}$  and  $\mathbf{P}_u^{(k_0)}$  that are respectively a lower bound and an upper

bound of  $\mathbf{P}$  (for example, one can choose  $\mathbf{P}_l^{(k_0)}$  to be identically 0 on  $\mathcal{Q}^0$  and  $\mathbf{P}_u^{(k_0)}$  to be identically 1 on  $\mathcal{Q}^0$ ). By Lemma 2, the iterated results at every  $k \leq k_0$  for the two initial conditions will provide a lower bound and an upper bound of  $\mathbf{P}_{c,\delta}^{(k_c+1)}$ , respectively, which also converge toward each other (hence to  $\mathbf{P}_{c,\delta}^{(k_c+1)}$  as well) as  $k \rightarrow -\infty$ . By running the iterations for the upper and lower bounds in parallel we can determine an approximation of  $\mathbf{P}_{c,\delta}^{(k_c+1)}$  within any accuracy.

*Remark 2.* As  $\delta \rightarrow 0$ , the size of the matrix  $\mathbf{A}$  becomes larger. Moreover, the ratio  $|\mathcal{Q}^0|^0/|\mathcal{Q}^0| \rightarrow 1$ . Hence  $\mathbf{A}$  will have an eigenvalue close to 1 whose corresponding eigenvector is close to  $(1, \dots, 1)$ . This causes slower convergence for the iteration (16) and numerical problems for the solution to the fixed point equation (17).  $\square$

### 2.5 Extension to the case when the initial state is uncertain

The procedure for estimating  $P_c$  can be easily extended to the case when the initial state  $S(0)$  is not known precisely.

Suppose that  $S(0)$  is described as a random variable with distribution  $\mu_S(s)$ ,  $s \in \mathcal{U} \setminus \mathcal{D}$ . Then, the probability of entering the unsafe set  $\mathcal{D}$  can be expressed as

$$P_c = \int_{\mathcal{U} \setminus \mathcal{D}} p_c(s) d\mu_S(s), \quad (18)$$

where  $p_c : \mathcal{U} \setminus \mathcal{D} \rightarrow [0, 1]$  is defined by

$$p_c(s) := P\{S \text{ hits } \mathcal{D} \text{ before hitting } \mathcal{U}^c \text{ within the time interval } T \mid S(0) = s\}.$$

For each  $s \in \mathcal{U} \setminus \mathcal{D}$ ,  $p_c(s)$  is the probability of entering the unsafe set  $\mathcal{D}$  over the time horizon  $T$  when  $S(0) = s$  and is exactly the quantity estimated with  $P_{c,\delta}^{(0)}$  in the iterative procedure proposed in Section 2.4. The integral (18) then reduces to a finite summation when approximating the map  $p_c$  with  $P_{c,\delta}^{(0)}$ .

## 3 Application to aircraft conflict prediction

In the current centralized ATM system, aircraft are prescribed to follow certain flight plans, and Air Traffic Controllers (ATCs) on the ground are responsible for ensuring aircraft safety by issuing trajectory specifications to the pilots. The flight plan assigned to an aircraft is “safe” if by following it the aircraft will not get into any conflict situation.

Conflict situations arise, for example, when an aircraft gets closer than a certain distance to another aircraft or it enters some forbidden region of the airspace. In the sequel, these conflicts are shortly referred to as “aircraft-to-aircraft conflict” and “aircraft-to-airspace conflict”, respectively.

The procedure used to prevent the occurrence of a conflict in ATM typically consists of two phases, namely, aircraft conflict detection and aircraft conflict resolution. Automated tools are currently being studied to support ATCs in performing these tasks. A comprehensive overview of the methods proposed in the literature for aircraft-to-aircraft conflict detection can be found in [18].

In automated conflict detection, models for predicting the aircraft future position are introduced and the possibility that a conflict would happen within a certain time horizon is evaluated based on these models ([34, 27, 28, 7]). If a conflict is predicted, then the aircraft flight plans are modified in the conflict resolution phase so as to avoid the actual occurrence of the predicted conflict. The cost of the resolution action in terms of, for example, delay, fuel consumption, deviation from originally planned itinerary, is usually taken into account when selecting a new flight plan ([10, 33, 23, 13, 17, 24, 35, 16]).

The conflict detection issue can be formulated as a probabilistic safety verification problem, where the objective is to evaluate if the flight plan assigned to an aircraft is “safe”. Safety can be assessed by estimating the probability that a conflict will occur over some look-ahead time horizon. In practice, once a prescribed threshold value of the probability of conflict is surpassed, an alarm of corresponding severity should be issued to the air traffic controllers/pilots to warn them on the level of criticality of the situation [34].

There are several factors that combined make this conflict analysis problem highly complicated, and as such impossible to solve analytically. Aircraft flight plans can be, in principle, arbitrary motions in the three dimensional airspace, and they are generally more complex than the simple planar linear motions assumed in [28, 8] when determining analytic expressions for the probability of an aircraft-to-aircraft conflict. Also, forbidden airspace areas may have an arbitrary shape, which can also change in time, as, for example, in the case of a storm that covers an area of irregular shape that evolves dynamically. Finally, and probably most importantly, the random perturbation to the aircraft motion is spatially correlated. Wind is a main source of uncertainty on the aircraft position, and if we consider two aircraft, the closer the aircraft, the larger the correlation between the wind perturbations. Although this last factor is known to be critical, it is largely ignored in the current literature on aircraft safety studies, probably because it is difficult to model and analyze. The methods proposed in the literature to compute the probability of conflict are generally based on the description of the aircraft future positions first proposed in [27]. In [27], each aircraft motion is described as a Gaussian random process whose variance grows in time, and the processes modeling the motions of different aircraft are assumed to be uncorrelated. However, this assumption may be unrealistic in practice, and can cause erroneous evaluations of the probability of conflict, since the correlation between the wind perturbations affecting the aircraft positions is stronger when two aircraft are closer to each other. To our knowledge, the first attempt to model

the wind perturbation to the aircraft motion for ATM applications was done in [22], which inspired this work.

The model introduced for predicting the aircraft future position incorporates the information on the aircraft flight plan, and takes into account the presence of wind as the main source of uncertainty on the aircraft actual motion. We address the general case when the aircraft might change altitude during its flight. Modeling altitude changes is important not only because the aircraft changes altitude when it is inside a Terminal Radar Approach Control (TRACON) area, but also because altitude changes can be used as resolution maneuvers to avoid, e.g., severe perturbation areas or conflict situations with other aircraft ([29],[21],[17]).

It is important to note that we do not address issues related to a possible discrepancy between the flight plan at the ATC level and that set by the pilot on board of the aircraft. Modeling this aspect would require a more complex stochastic hybrid model than the one introduced here, where the hybrid component of the system is mainly due to changes in the aircraft dynamics at the way-points prescribed by their flight plan. Detecting situation awareness errors in fact requires modeling ATC and pilots by hybrid systems, and building an observer for the overall hybrid system obtained by composing the hybrid models of the agents and the aircraft.

The results illustrated here have appeared in [9], [11], [12], and [14].

### 3.1 Model of the aircraft motion

In this section we introduce a kinematic model of the aircraft motion to predict the aircraft future position during the time interval  $T = [0, t_f]$ .

The airspace and the aircraft position at time  $t \in T$  are  $\mathbb{R}^3$  and  $X(t) \in \mathbb{R}^3$ , respectively. We assume that the flight plan assigned to the aircraft is specified in terms of a velocity profile  $u : T \rightarrow \mathbb{R}^3$ , meaning that at time  $t \in T$  the aircraft plans to fly at a velocity  $u(t)$ . Since, according to the common practice in ATM systems, aircraft are advised to travel at constant speed piecewise linear motions specified by a series of way-points, the velocity profile  $u$  is taken to be a piecewise constant function.

We suppose that the main source of uncertainty in the aircraft future position during the time interval  $T$  is the wind which affects the aircraft motion by acting on the aircraft velocity. The wind contribution to the velocity of the aircraft is due to the *wind speed*. Note that here we adopt the ATM terminology and use the word ‘speed’ for the velocity vector.

The wind speed can be further decomposed into two components: i) a deterministic term representing the nominal wind speed, which may depend on the aircraft location and time  $t$ , and is assumed to be known to the ATC through measurements or forecast; and ii) a stochastic term representing the effect of air turbulence and errors in the wind speed measurements and forecast.

As a result of the above discussion, the position  $X$  of the aircraft during the time horizon  $T$  is governed by the following stochastic differential equation:

$$dX(t) = u(t)dt + f(X, t)dt + \Sigma(X, t)dB(X, t), \quad (19)$$

initialized with the aircraft current position  $X(0)$ .

We next explain the different terms appearing in equation (19).

First of all,  $f : \mathbb{R}^3 \times T \rightarrow \mathbb{R}^3$  is a time-varying vector field on  $\mathbb{R}^3$ : for a fixed  $(x, t) \in \mathbb{R}^3 \times T$ ,  $f(x, t)$  represents the nominal wind speed at position  $x$  and at time  $t$ . We call  $f$  the *wind field*.

$B(\cdot, \cdot)$  is a time-varying random field on  $\mathbb{R}^3 \times T$  modeling (the integral of) air turbulence perturbations to aircraft velocity as well as wind speed forecast errors. It can be thought of as the time integral of a Gaussian random field correlated in space and uncorrelated in time. Formally,  $B(\cdot, \cdot)$  has the following properties:

- i)* for each fixed  $x \in \mathbb{R}^3$ ,  $B(x, \cdot)$  is a standard 3-dimensional Brownian motion. Hence  $dB(x, t)/dt$  can be thought of as a 3-dimensional white noise process;
- ii)*  $B(\cdot, \cdot)$  is time increment independent. This implies, in particular, that the collections of random variables  $\{B(x, t_2) - B(x, t_1)\}_{x \in \mathbb{R}^3}$  and  $\{B(x, t_4) - B(x, t_3)\}_{x \in \mathbb{R}^3}$  are independent for any  $t_1, t_2, t_3, t_4 \in T$ , with  $t_1 \leq t_2 \leq t_3 \leq t_4$ ;
- iii)* for any  $t_1, t_2 \in T$  with  $t_1 \leq t_2$ ,  $\{B(x, t_2) - B(x, t_1)\}_{x \in \mathbb{R}^3}$  is an (uncountable) collection of Gaussian random variables with zero mean and covariance

$$E\{[B(x, t_2) - B(x, t_1)][B(y, t_2) - B(y, t_1)]^T\} = \rho(x-y)(t_2 - t_1)I_3, \quad \forall x, y \in \mathbb{R}^3,$$

where  $I_3$  is the 3-by-3 identity matrix, and  $\rho : \mathbb{R}^3 \rightarrow \mathbb{R}$  is a continuous function with  $\rho(0) = 1$  and  $\rho(x)$  decreases to zero as  $x \rightarrow \infty$ . In addition,  $\rho$  has to be non-negative definite in the sense that the  $k$ -by- $k$  matrix  $[\rho(x_i - x_j)]_{i,j=1}^k$  is non-negative definite for arbitrary  $x_1, \dots, x_k \in \mathbb{R}^3$  and positive integer  $k$ . See [1] for other equivalent conditions of this non-negative definite requirement.

*Remark 3.* Typically the wind field  $f$  is supposed to satisfy some continuity property. This condition, together with the monotonicity assumption on the spatial correlation function  $\rho$ , is introduced to model the fact that the closer two points in space, the more similar the wind speeds at those points, and, as the two points move farther away from each other, their wind speeds become more and more independent.

The spatial correlation function  $\rho : \mathbb{R}^3 \rightarrow \mathbb{R}$  can be taken to be  $\rho(x) = \exp(-c_h \|x\|_h - c_v \|x\|_v)$  for some  $c_v \geq c_h > 0$ , where the subscripts  $h$  and  $v$  stand for “horizontal” and “vertical”, and  $\|(x_1, x_2, x_3)\|_h := \sqrt{x_1^2 + x_2^2}$  and  $\|(x_1, x_2, x_3)\|_v := |x_3|$  for any  $(x_1, x_2, x_3) \in \mathbb{R}^3$ . This is to model the fact that the wind correlation in space is weaker in the vertical direction.

Exponentially decaying spatial correlation functions are a popular choice for random field models in geostatistics [15]. This choice is actually suitable for ATM applications. In [5], the wind field prediction made by the Rapid Update Cycle (RUC [3]) developed at the National Oceanic and Atmospheric Administration (NOAA) Forecast System Laboratory (FOL) is compared with the empirical data collected by the Meteorological Data Collection Reporting System (MDCRS) near Denver International Airport. The result of this comparison is that the spatial correlation statistics of the wind field prediction errors is adequately described by an exponentially decaying function of the horizontal separation.

As a random field,  $B(\cdot, \cdot)$  is Gaussian, stationary in space (its finite dimensional distributions remain unchanged when the origin of  $\mathbb{R}^3$  is shifted), and isotropic in the horizontal directions (its finite dimensional distributions are invariant with respect to changes of orthonormal coordinates in the horizontal directions).

Finally,  $\Sigma : \mathbb{R}^3 \times T \rightarrow \mathbb{R}^{3 \times 3}$  modulates the variance of the random perturbation to the aircraft velocity. We assume that  $\Sigma(\cdot, \cdot)$  is a constant diagonal matrix  $\Sigma$  given by  $\Sigma := \text{diag}(\sigma_h, \sigma_h, \sigma_v)$ , for some constant  $\sigma_h, \sigma_v > 0$ . Note that after the modulation of  $\Sigma$  the random contribution of the wind to the aircraft velocity remains isotropic horizontally. However, its variance in the vertical direction can be different from that in the horizontal ones.

Equation (19) can then be rewritten as

$$dX(t) = u(t)dt + f(X, t)dt + \Sigma dB(X, t) \quad (20)$$

with initial condition  $X(0)$ .

Based on model (20) of the aircraft motion, we shall derive the equations to study the aircraft-to-aircraft and aircraft-to-airspace problems.

Note that this simplified model of the aircraft motion does not take into account the feedback control action of the flight management system (FMS), which tries to reduce the tracking error with respect to the planned trajectory. However, the algorithm described based on this model can be extended to address also the case when a model of the FMS is included.

### 3.2 Aircraft-to-aircraft conflict problem

Consider two aircraft, say “aircraft 1” and “aircraft 2”, flying in the same region of the airspace during the time interval  $T = [0, t_f]$ .

According to the ATM definition, a two-aircraft encounter is conflict-free if the two aircraft are either at a horizontal distance greater than  $r$  or at a vertical distance greater than  $H$  during the whole duration of the encounter, where  $r$  and  $H$  are prescribed quantities [29]. Currently,  $r = 5$  nautical miles (nmi) for en-route airspace and  $r = 3$  nmi inside the TRACON area, whereas  $H = 1000$  feet (ft). If the two aircraft get closer than  $r$  horizontally and  $H$  vertically at some  $t \in T$ , then, an aircraft-to-aircraft conflict occurs.

Denote the position of aircraft 1 and aircraft 2 by  $X_1$  and  $X_2$ , respectively. Based on (20), the evolutions of  $X_1(\cdot)$  and  $X_2(\cdot)$  over the time interval  $T$  are governed by

$$dX_1(t) = u_1(t)dt + f(X_1, t)dt + \Sigma dB(X_1, t), \quad (21)$$

$$dX_2(t) = u_2(t)dt + f(X_2, t)dt + \Sigma dB(X_2, t), \quad (22)$$

starting from the initial positions  $X_1(0)$  and  $X_2(0)$ .

The probability of conflict can be expressed in terms of the relative position  $Y := X_2 - X_1$  of the two aircraft as

$$P\{Y(t) \in \mathcal{D} \text{ for some } t \in T\}, \quad (23)$$

where  $\mathcal{D} \in \mathbb{R}^3$  is the closed cylinder of radius  $r$  and height  $2H$  centered at the origin.

### Affine case

Let the wind field  $f(x, t)$  be affine in  $x$ , i.e.,

$$f(x, t) = R(t)x + d(t), \quad \forall x \in \mathbb{R}^3, t \in T,$$

where  $R : T \rightarrow \mathbb{R}^{3 \times 3}$  and  $d : T \rightarrow \mathbb{R}^3$  are continuous functions. We shall show that in this case we can refer to a simplified model for the two-aircraft system to compute the probability of conflict.

Since the positions of the two aircraft,  $X_1$  and  $X_2$ , are governed by equations (21) and (22), by subtracting (21) from (22), we have that the relative position  $Y = X_2 - X_1$  of aircraft 1 and aircraft 2 is governed by

$$dY(t) = v(t)dt + R(t)Y(t)dt + \Sigma d[B(X_2, t) - B(X_1, t)], \quad (24)$$

where  $v := u_2 - u_1$  is the nominal relative velocity.  $B(\cdot, \cdot)$  can be rewritten in the Karthunen-Loeve expansion as

$$B(x, t) = \sum_{n=0}^{\infty} \sqrt{\lambda_n} \phi_n(x) B_n(t),$$

where  $\{B_n(t)\}_{n \geq 0}$  is a series of independent three-dimensional standard Brownian motions, and  $\{(\lambda_n, \phi_n(x))\}_{n \geq 0}$  is a complete set of eigenvalue and eigenfunction pairs for the integral operator  $\phi(x) \mapsto \int_{\mathbb{R}^3} \rho(s-x)\phi(s) ds$ , i.e.,

$$\begin{cases} \lambda_n \phi_n(x) = \int_{\mathbb{R}^3} \rho(s-x)\phi_n(s) ds, \\ \rho(x-y) = \sum_{n=0}^{\infty} \lambda_n \phi_n(x)\phi_n(y), \end{cases} \quad \forall x, y \in \mathbb{R}^3. \quad (25)$$

Fix  $x_1, x_2 \in \mathbb{R}^3$  and let  $y = x_2 - x_1$ . Define

$$Z(t) := B(x_2, t) - B(x_1, t) = \sum_{n=0}^{\infty} \sqrt{\lambda_n} [\phi_n(x_2) - \phi_n(x_1)] B_n(t). \quad (26)$$

$Z(t)$  is a Gaussian process with zero mean and covariance

$$E\{[Z(t_2) - Z(t_1)][Z(t_2) - Z(t_1)]^T\} = 2[1 - \rho(y)](t_2 - t_1)I_3, \quad \forall t_1 \leq t_2,$$

where the last equation follows from (25) and the fact that  $\rho(0) = 1$ . Note also that  $Z(0) = 0$ . Therefore, in terms of distribution we have

$$Z(t) \stackrel{d}{=} \sqrt{2[1 - \rho(y)]} W(t), \quad (27)$$

where  $W(t)$  is a standard 3-dimensional Brownian motion.

As a result, (24) can then be approximated weakly by

$$dY(t) = v(t)dt + R(t)Y(t)dt + \sqrt{2[1 - \rho(Y)]}\Sigma dW(t). \quad (28)$$

By this we mean that the stochastic process  $Y(t) = X_2(t) - X_1(t)$  obtained by subtracting the solution to (21) from the solution to (22) initialized respectively with  $X_1(0)$  and  $X_2(0)$  has the same distribution as the solution to (28) initialized with  $Y(0) = X_2(0) - X_1(0)$ .

Equation (28) is a particular case of (1) with  $S = Y$ ,  $\Gamma = \Sigma$ ,  $a(y, t) = v(t) + R(t)y$ , and  $b(y) = \sqrt{2[1 - \rho(y)]}I$ , with the discontinuity in  $a$  caused by the discontinuity in the aircraft flight plan at the prescribed timed way-points. Given that  $b(y) = \beta(y)I$  with  $\beta(y) := \sqrt{2[1 - \rho(y)]}$ , we can apply Algorithm 1 to estimate the probability of conflict (23) with the transition probabilities of the approximating Markov chain given by (7).

#### *Examples of 2-D aircraft-to-aircraft conflict prediction*

We consider two aircraft flying in the same region of the airspace at a fixed altitude. The two-aircraft system is described by equations (21) and (22), with  $X_1$  and  $X_2$  denoting the two aircraft positions and taking values in  $\mathbb{R}^2$ . Note that the model described in Section 3.1 refers to the 3D flight case, where the aircraft positions take value in  $\mathbb{R}^3$ . However, it can be easily reformulated for the 2D case by minor modifications. In the 2D case, a conflict occurs when  $Y = X_2 - X_1$  enters the unsafe set  $\mathcal{D} = \{y \in \mathbb{R}^2 : \|y\| \leq r\}$ .

In the following examples the safe distance  $r$  is set equal to 3, whereas the spatial correlation function  $\rho$  and matrix  $\Sigma$  are given by  $\rho(y) = \exp(-c\|y\|)$ ,  $y \in \mathbb{R}^2$  and  $\Sigma = \sigma I$ , where  $c$  and  $\sigma$  are positive constants. In all the plots of the estimated probability of conflict, the reported level curves refer to values 0.1, 0.2, ..., 0.9.

Unless otherwise stated, in all of the examples in this subsection we use the following parameters:

The time interval of interest is  $T = [0, 40]$ . The relative velocity of the two aircraft during the time horizon  $T$  is given by

$$v(t) = \begin{cases} (2, 0), & 0 \leq t < 10; \\ (0, 1), & 10 \leq t < 20; \\ (2, 0), & 20 \leq t \leq 40. \end{cases}$$

The parameter  $\sigma$  is equal to 1.

Based on the values of  $T$  and  $v(t)$ ,  $t \in T$ , the domain  $\mathcal{U}$  is chosen to be the open rectangle  $(-80, 10) \times (-40, 10)$ . The grid size is  $\delta = 1$ , hence the sampling time interval is  $\Delta t = \lambda \delta^2 = (4\sigma^2)^{-1} \delta^2 = 0.25$ .

$\lambda$  appearing in (7) is set equal to  $\lambda = (4\sigma^2)^{-1}$ .

*Example 1.* We consider the case when the wind field is identically zero:  $f(x, t) = 0$ , for all  $t \in T$ ,  $x \in \mathbb{R}^2$ . We set  $c = 0.2$  in the spatial correlation function  $\rho$ . In Figure 2 we plot the level curves of the estimated probability of conflict over the time horizon  $[t, t_f]$  as a function of the aircraft relative position at time  $t$ . As one can expect, the probability of conflict over  $[t, t_f]$  takes higher values along the nominal path, which is the path traced by a point that starts from the origin at time  $t_f = 40$  and moves backward in time according to the nominal relative velocity  $v(\cdot)$  until time  $t$ . Furthermore, as the relative positions between the aircraft at time  $t$  move farther away from that path, the probability of conflict decreases. Experiments (not reported here) show that the smaller the variance parameter  $\sigma$ , the faster this decrease.

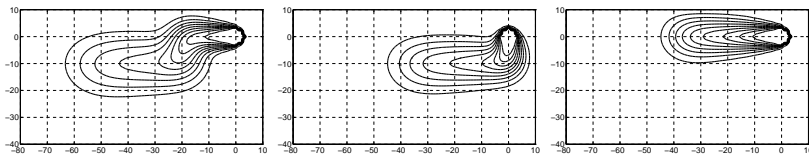


**Fig. 2.** Example 1. Level curves of the estimated probability of conflict over the time horizon  $[t, 40]$  ( $c = 0.2$ ). Left:  $t = 0$ . Center:  $t = 10$ . Right:  $t = 20$ .

*Example 2.* This example differs from the previous one only in the value of  $c$ , which is now set equal to  $c = 0.05$ . Then  $\rho(y) = \exp(-0.05\|y\|)$  for  $y \in \mathbb{R}^2$ , which decreases much more slowly than in the previous case as  $\|y\|$  increases. Since  $\rho$  characterizes the strength of spatial correlation in the random field  $B(\cdot, \cdot)$ , this means that the random components of the wind contributions to the two aircraft velocities tend to be more correlated to each other than in Example 1. In Figure 3, we plot the level curves of the estimated probability of conflict over  $[t, t_f]$  in the cases  $t = 0$ ,  $t = 10$ , and  $t = 20$ . One can see that, compared to the plots in Figure 2, the regions with higher probability of conflict in Figure 3 are more concentrated along the nominal path, which is especially evident near the origin. In a sense, this implies that the current approaches to estimating the probability of conflict, based on the assumption of independent wind perturbations to the aircraft velocities, could

be pessimistic. The intuitive explanation of this phenomenon is that random wind perturbations to the aircraft velocities with larger correlations are more likely to cancel each other, resulting in more predictable behaviors and hence smaller probability of conflict.

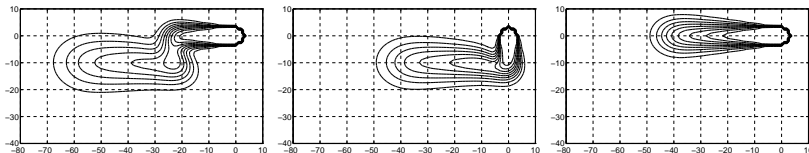


**Fig. 3.** Example 2. Level curves of the estimated probability of conflict over the time horizon  $[t, 40]$  ( $c = 0.05$ ). Left:  $t = 0$ . Center:  $t = 10$ . Right:  $t = 20$ .

*Example 3.* In this example, we choose  $c = 0.05$  as in Example 2. However, we assume that there is a nontrivial affine wind field  $f$  defined by

$$f(x, t) = R(t)[x - z(t)], \quad x \in \mathbb{R}^2, \quad t \in [0, 40],$$

where

$$R(t) \equiv \frac{1}{50} \begin{bmatrix} 0 & 1 \\ -1 & 0 \end{bmatrix}, \quad z(t) = \begin{bmatrix} 3t \\ t^2/5 \end{bmatrix}.$$

The wind field  $f$  can be viewed as a windstorm swirling clockwise, whose center  $z(t)$  accelerates along a curve during  $T$ . In fact, the choice of  $z(t)$  will have no effect on the probability of conflict since it does not affect the aircraft relative position. In the first row of Figure 4, we plot the wind field  $f$  in the region  $[-100, 200] \times [-100, 200]$  at the time instant  $t = 0$  and the level curves of the estimated probability of conflict over  $[t, t_f]$ , at  $t = 0$ . In the second and third rows we represent similar plots for  $t = 10$  and  $t = 20$ , respectively. One can see that, compared to the results in Figure 3, the regions with high probability of conflict are “bent” counterclockwise, and the farther away from the origin, the more the bending. This is because the net effect of the wind field  $f$  on the relative velocity  $v$  of the two aircraft is  $RY$ , which points clockwise when the relative position  $Y$  is in the third quarter of the Cartesian plane.

*Example 4.* Suppose now that in Example 3 we change the ending epoch  $t_f$  from 40 to infinity, and assume that the relative velocity  $v$  remains constant and equal to  $(2, 0)^T$  from time 20 on. For this infinite horizon problem, we can obtain an estimate of the probability of conflict at time  $t = 0, 10, 20$  as drawn from top to bottom in Figure 5. Note that, unlike in the previous examples, the regions with high probability of conflict extend outside the domain  $\mathcal{U}$  and are truncated. This is the price we pay to evaluate numerically the probability of conflict.

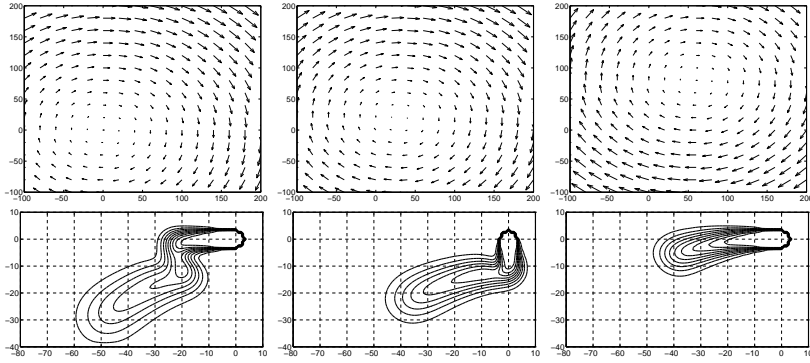


**Fig. 4.** Example 3. Wind field at time  $t$ , and level curves of the estimated probability of conflict over the time horizon  $[t, 40]$  ( $c = 0.05$ ). Left:  $t = 0$ . Center:  $t = 10$ . Right:  $t = 20$ .

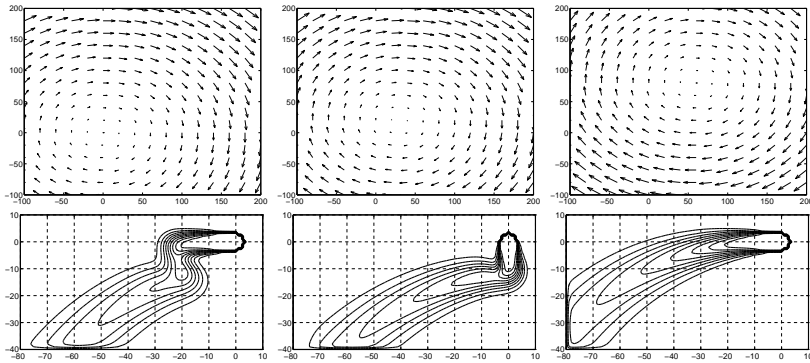


**Fig. 5.** Example 4. Wind field at time  $t$ , and level curves of the estimated probability of conflict over the time horizon  $[t, \infty]$  ( $c = 0.05$ ). Left:  $t = 0$ . Center:  $t = 10$ . Right:  $t = 20$ .

*Examples of 3-D aircraft-to-aircraft conflict prediction*

We consider a two-aircraft encounter where the aircraft positions  $X_1$  and  $X_2$  take values in  $\mathbb{R}^3$  and are governed by equations (21) and (22).

The wind field  $f$  is assumed to be identically zero. A conflict occurs when  $Y = X_2 - X_1$  enters the unsafe set  $\mathcal{D} = \{y \in \mathbb{R}^2 : \|y\|_h \leq r, \|y\|_v \leq H\}$ . Here we set  $r = 3$  and  $H = 1$ .

We consider the case when  $\rho(y) = \exp(-c_h \|y\|_h - c_v \|y\|_v)$ ,  $y \in \mathbb{R}^3$ , with  $c_h$  and  $c_v$  positive constants, and the matrix  $\Sigma$  is given by  $\Sigma = \text{diag}(\sigma_h, \sigma_h, \sigma_v)$ , where  $\sigma_h = 1$  and  $\sigma_v = 0.5$ .

We evaluate the probability that a conflict situation occurs within the time horizon  $T = [0, 40]$ , when the relative velocity of the two aircraft during  $T$  is given by

$$v(t) = \begin{cases} (2, 0, 0), & 0 \leq t < 5; \\ (0, 1, 1), & 5 \leq t \leq 10. \end{cases}$$

Based on the values taken by  $T$ ,  $v(\cdot)$ ,  $r$  and  $H$ , we choose the domain  $\mathcal{U}$  to be  $\mathcal{U} = (-30, 15) \times (-15, 10) \times (-15, 10)$ . We set the discretization step size  $\delta = 1$ , and  $\lambda = (6\sigma_h^2)^{-1} = 1/6$ . Thus  $\Delta t = \lambda\delta^2 = 1/6$ .

Figure 6 represents the estimated probability of conflict over the time horizon  $[0, 10]$  as a function of the relative position of the two aircraft at time  $t$ . The plots refer to the cases when  $c_h = 0.2$ ,  $c_v = 0.5$  and  $c_h = 0.05$ ,  $c_v = 0.05$  shown column-wise from left to right. In each column, we have the three dimensional isosurface at value 0.2 of the estimated probability of conflict viewed from different angles. The relevance of isosurfaces is that, in practice, once the relative position of the two aircraft is within the isosurface at a prescribed threshold value, an alarm of corresponding severity should be issued to the pilots to warn them on the level of criticality of the situation ([34]).

Note that when the parameters  $c_h$  and  $c_v$  of the spatial correlation function  $\rho$  are set equal to  $c_h = c_v = 0.05$ , the wind spatial correlation is increased. As a consequence of this fact, the isosurface at 0.2 concentrates more tightly along the deterministic path that leads to a conflict, and it extends longer as well.

### General case

If no assumption is made on the wind field  $f(x, t)$ , to compute the probability of conflict (23), it no longer suffices to consider only the relative position of the two aircraft as in the affine case. Instead, we have to keep track of the two aircraft positions.

Define

$$\hat{X} = \begin{bmatrix} X_1 \\ X_2 \end{bmatrix} \in \mathbb{R}^6.$$

Then equations (21) and (22) can be written in terms of  $\hat{X}$  as a single equation:

$$d\hat{X}(t) = \hat{u}(t)dt + \hat{f}(\hat{X}, t)dt + \hat{\Sigma}d\hat{B}(\hat{X}, t), \quad (29)$$

where we set

$$\hat{\Sigma} := \begin{bmatrix} \Sigma & 0 \\ 0 & \Sigma \end{bmatrix}, \quad \hat{u}(t) := \begin{bmatrix} u_1(t) \\ u_2(t) \end{bmatrix}, \quad \hat{f}(\hat{X}, t) = \begin{bmatrix} f(X_1, t) \\ f(X_2, t) \end{bmatrix}, \quad \hat{B}(\hat{X}, t) := \begin{bmatrix} B(X_1, t) \\ B(X_2, t) \end{bmatrix}.$$

Fix  $\hat{x} \in \mathbb{R}^6$ . Let  $\hat{Z}(t) := \hat{\Sigma} \hat{B}(\hat{x}, t)$ .  $\{\hat{Z}(t), t \geq 0\}$  is a Gaussian process with zero mean and covariance

$$E[\hat{Z}(t)\hat{Z}(t)^T] = \begin{bmatrix} t I_3 & \hat{\rho}(\hat{x}) t I_3 \\ \hat{\rho}(\hat{x}) t I_3 & t I_3 \end{bmatrix} \hat{\Sigma}^2,$$

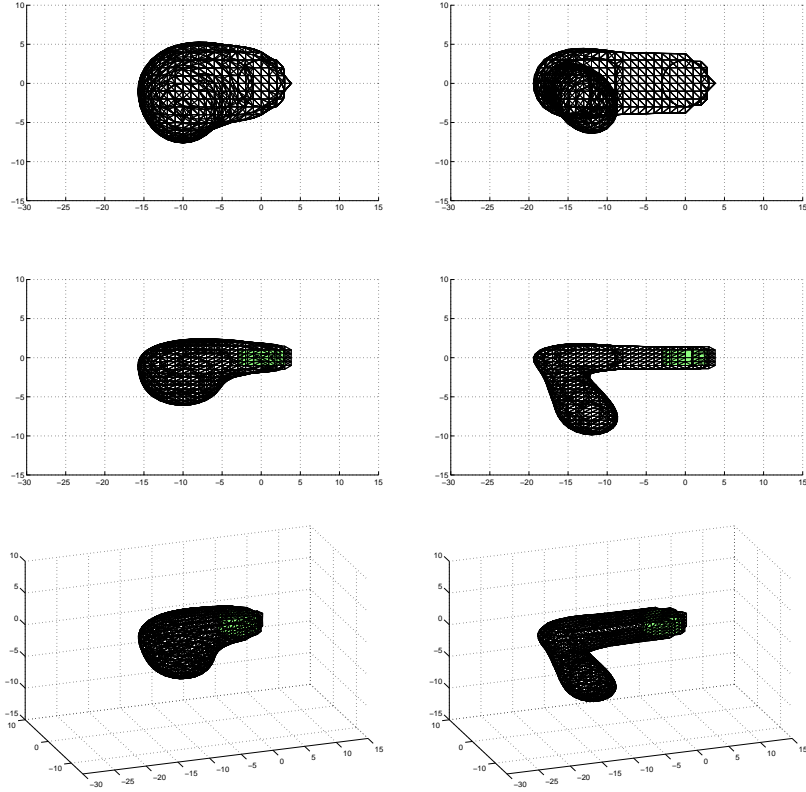


**Fig. 6.** Estimated probability of conflict over the time horizon  $[0, 10]$ : isosurface at value 0.2. Left:  $c_h = 0.2$  and  $c_v = 0.5$ . Right:  $c_h = 0.05$  and  $c_v = 0.05$ . First row: top view. Second row: side view. Third row: three dimensional plot.

with  $\hat{\rho}(\hat{x}) := \rho(x_1 - x_2)$ , with  $\hat{x} := (x_1, x_2)$ . Analogously to the previous section, in terms of distribution,  $\hat{Z}(t) \stackrel{d}{\simeq} \sigma(\hat{x})\hat{\Sigma}\hat{W}(t)$ , where  $\hat{W}(t)$  is a standard Brownian motion in  $\mathbb{R}^6$ , and

$$\sigma(\hat{x}) := \begin{bmatrix} I_3 & \hat{\rho}(\hat{x}) I_3 \\ \hat{\rho}(\hat{x}) I_3 & I_3 \end{bmatrix}^{1/2} \in \mathbb{R}^{6 \times 6}.$$

As a result, (29) becomes

$$d\hat{X}(t) = \hat{u}(t)dt + \hat{f}(\hat{X}, t)dt + \sigma(\hat{X})\hat{\Sigma}d\hat{W}(t). \quad (30)$$

Equation (29) is a particular case of (1) with  $S = \hat{X}$ ,  $\Gamma = \hat{\Sigma}$ ,  $a(\hat{x}, t) = \hat{u}(t) + \hat{f}(\hat{x}, t)$ , and  $b(\hat{x}) = \sigma(\hat{x})$ . In this case, we can apply Algorithm 1 to estimate the probability of conflict (23) with the transition probabilities of the approximating Markov chain given by (9).

*Example 5.* In this example, we consider two aircraft flying in the same region of the airspace at a fixed altitude. The safe distance  $r$  is set equal to 3, whereas the spatial correlation function  $\rho$  and matrix  $\Sigma$  are given by  $\rho(y) = \exp(-c\|y\|)$ ,  $y \in \mathbb{R}^2$  and  $\Sigma = \sigma I$ , where  $c = 1$  and  $\sigma = 2$ .

The time interval of interest is  $T = [0, 20]$ . The velocities of the two aircraft during the time horizon  $T$  are supposed to be constant and given by

$$u_1(t) = \begin{bmatrix} 4 \\ 0 \end{bmatrix}, \quad u_2(t) = \begin{bmatrix} 2 \\ 0 \end{bmatrix}, \quad 0 \leq t \leq 20.$$

The wind field is assumed to depend only on the spatial coordinate  $x \in \mathbb{R}^2$  as follows

$$f(x, t) = \begin{bmatrix} \frac{\exp([x]_1+20)/2-1}{\exp([x]_1+20)/2+1} \\ 0 \end{bmatrix}.$$

where  $[x]_1$  is the first component of  $x$ . Under this wind field model, the wind direction is along the  $[x]_1$  axis from right to left on the half-plane with  $[x]_1 < -20$ , and from left to right on the half-plane with  $[x]_1 > -20$ . The maximal strength  $\|f(x, t)\|$  of the wind is 1, which is achieved when  $[x]_1 \rightarrow \pm\infty$ .

Based on the values taken by  $T$ , and  $u_1(t), u_2(t)$ ,  $t \in T$ , we set  $\mathcal{U} := \mathcal{U}_1 \times \mathcal{U}_2$ , with  $\mathcal{U}_1$  and  $\mathcal{U}_2$  open rectangles  $\mathcal{U}_1 = (-100, 30) \times (-24, 24)$  and  $\mathcal{U}_2 = (-60, 80) \times (-16, 16)$ . Finally, we set  $\lambda = (2\sigma^2)^{-1} = 0.125$  and  $\delta = 1.5$ , so that  $\Delta t = \lambda\delta^2 = 9/32$ .

In Figure 7, we plot the level curves of the estimated probability of conflict as a function of the initial position of aircraft 1, for five different initial positions of aircraft 2:  $(-40, 0)$ ,  $(-30, 0)$ ,  $(-20, 0)$ ,  $(0, 0)$ , and  $(20, 0)$ , moving from top to bottom in the figure. On each row, the figure on the left side corresponds to the probability of conflict as computed by Algorithm 1. Since we use a relative coarse grid  $\delta = 1.5$ , the level curves are not smooth. For better visualization, we plot on the right side the level curves of a smoothed version of the probability of conflict maps, whose value at each grid point  $w \in \mathcal{U}_1 \cap \delta\mathbb{Z}^2$  is the average value of the probability of conflict at  $w$  and its four immediate neighboring points  $w_{1-}$ ,  $w_{1+}$ ,  $w_{2-}$ ,  $w_{2+}$ . In effect, this is equivalent to passing the original probability of conflict map through a low pass filter. This also corresponds to assuming that there is uncertainty in the initial position of aircraft 1, such that it is equally probable that aircraft 1 occupies its nominal position and the four immediate neighboring grid points.

In the reported example, we see that, unlike the affine wind field case, the probability of conflict in general depends on the initial positions of both aircraft, not just on their initial relative position. If the probability of conflict would depend only on the aircraft initial relative position, then the level curves in the plots of Figure 7 will be all identically shaped and one could be obtained from another by translation of an amount given by the difference between the

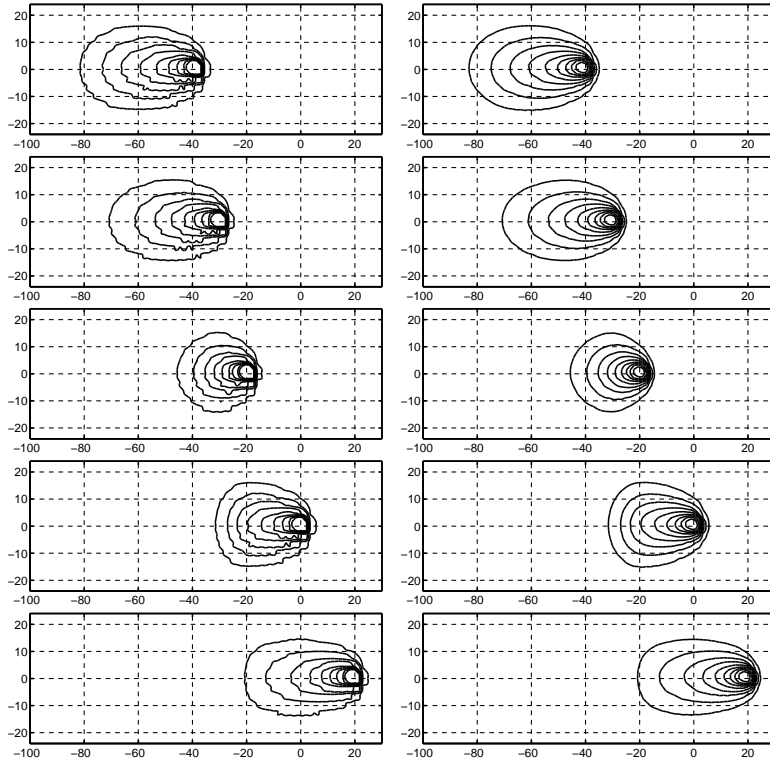


**Fig. 7.** Example 5. Left: Level curves of the estimated probability of conflict over the time horizon  $[0, 20]$  as a function of the initial position of aircraft 1 for fixed initial position of aircraft 2 (from top to bottom:  $(-40, 0)$ ,  $(-30, 0)$ ,  $(-20, 0)$ ,  $(0, 0)$ , and  $(20, 0)$ ). Right: Level curve of a smooth version of the corresponding quantity on the left. (Non-affine wind field)

corresponding initial positions of aircraft 2, which is obviously not the case in Figure 7.

The dependence of the probability of conflict on the initial positions of both aircraft rather than simply their relative position is more eminent at those places where there is a large acceleration (or deceleration) in wind components, i.e., at those places with higher degree of nonlinearity in the wind field. If the nonlinearity of the wind field is relatively small, the two-aircraft system could be described in terms of the their relative position, significantly reducing the computation time.

### 3.3 Aircraft-to-airspace conflict problem

An aircraft-to-airspace conflict occurs when the aircraft enters a forbidden area of the airspace. For a variety of reasons, an aircraft trajectory is con-

strained to limited spaces during a flight. Large sectors of airspace over Europe are “no-go” because of, for example, Special Use Airspace (SUA) areas in the military airspace or separation buffers around strategically important objects. Airspace restrictions can also originate dynamically due to severe weather conditions or high traffic congestion causing some airspace area to exceed its maximal capacity. The management of air traffic as density increases around the restricted areas is then crucial to avoid aircraft-to-airspace conflicts.

Consider an aircraft flying in some region of the airspace. An aircraft-to-airspace conflict occurs if the aircraft enters the prohibited area within the look-ahead time horizon  $T$ . If this area can be described by a set  $\mathcal{D} \subset \mathbb{R}^3$ , then this problem can be formulated as the estimation of the probability

$$P\{X(t) \in \mathcal{D} \text{ for some } t \in T\} \quad (31)$$

where  $X(t)$  is the aircraft position at time  $t \in T$  and is obtained by (20) initialized with  $X(0)$ .

Note that we are considering a single aircraft, and, for each fixed  $x \in \mathbb{R}^n$ ,  $B(x, \cdot)$  is a standard 3-dimensional Brownian motion, and  $B(\cdot, \cdot)$  is time increment independent and stationary. We can then replace  $B(\cdot, \cdot)$  with a standard Brownian motion  $W(\cdot)$ , and refer to

$$dX(t) = u(t)dt + f(X, t)dt + \Sigma dW(t), \quad (32)$$

initialized with  $X(0)$ , for the purpose of computing the probability in (31).

Equation (32) is a particular case of (1) with  $S = X$ ,  $\Gamma = \Sigma$ ,  $a(x, t) = u(t) + f(x, t)$ , and  $b(x) = I$ . In this case, we can apply Algorithm 1 to estimate the probability of conflict (23) with the transition probabilities of the approximating Markov chain given by (7).

*Example 6.* Suppose that an aircraft is flying along the  $x_1$ -axis while climbing up at an accelerated rate according to the flight plan  $u(t) = (3/2, 0, 2t/75)$ ,  $t \in T = [0, 15]$ . The wind field  $f$  is assumed to be identically zero. The matrix  $\Sigma$  is given by  $\Sigma = \text{diag}(\sigma_h, \sigma_h, \sigma_v)$ , where  $\sigma_h = 1$  and  $\sigma_v = 0.5$ .

Consider a prohibited airspace area  $\mathcal{D}$  given by the union of two ellipsoids specified by  $\{(x_1, x_2, x_3) \in \mathbb{R}^3 : 2(x_1 + 4)^2 + (x_2 - 4)^2 + 10x_3^2 \leq 9\}$  and  $\{(x_1, x_2, x_3) \in \mathbb{R}^3 : x_1^2 + 2(x_2 + 5)^2 + 10x_3^2 \leq 16\}$ , in the  $(x_1, x_2, x_3)$  Cartesian coordinate system with  $x_3$  representing the flight level.

Figure 8 shows the plots of the isosurface at value 0.2 of the probability of conflict as a function of the aircraft initial position, at time  $t = 0$ ,  $t = 5$ , and  $t = 10$ , viewed from three different angles. The probability of conflict is estimated through Algorithm 1 with  $\mathcal{U} = (-38, 6) \times (-15, 11) \times (-6, 3)$  and  $\delta = 1$ .

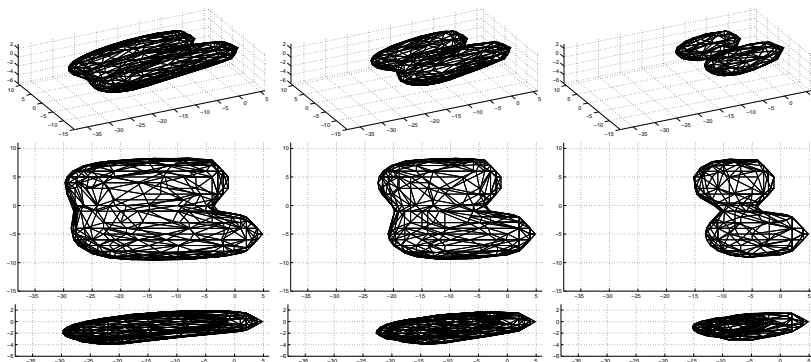


**Fig. 8.** Estimated probability of conflict over the time horizon  $[t, 15]$ : isosurface at value 0.2. Left:  $t = 0$ . Center:  $t = 5$ . Right:  $t = 10$ . First row: 3D plot. Second row: top view. Third row: side view.

## 4 Conclusions

In this work, we describe a novel grid-based method for estimating the probability that the trajectories of a system governed by a stochastic differential equation with time-driven jumps will enter some target set during some possibly infinite look-ahead time horizon. The distinguishing feature of the proposed method is that it is based on a Markov chain approximation scheme, integrating a backward reachability computation procedure.

This method is applied to estimate the probability that two aircraft flying in the same region of the airspace get closer than a certain safety distance and the probability that an aircraft enters a forbidden airspace area. The intended application is aircraft conflict detection, with the final objective of supporting air traffic controllers in detecting potential conflict situations so as to improve the efficiency of the air traffic management system in terms of airspace usage.

It is worth noticing that, though we provide as an application example air traffic control, our results may have potentials in other safety-critical contexts, where the safety verification problem can be reformulated as that of verifying if a given stochastic system trajectories will eventually enter some unsafe set.

Grid-based methods are generally computationally intensive. On the other hand, the outcome of the proposed grid-based algorithm is a map that associates to each admissible initial condition of the system the corresponding estimate of the probability of entering the unsafe set, which could be used not only for detecting an unsafe situation, but also for designing an appropriate action to timely steer the system outside the unsafe set. One could, for example, force the system to slide along a certain isosurface depending on the trust level.

## References

1. R.J. Adler. *The Geometry of Random Fields*. John Wiley & Sons, 1981.
2. R. Alur, T. Henzinger, G. Lafferriere, and G.J. Pappas. Discrete abstractions of hybrid systems. *Proceedings of the IEEE*, 88(2):971–984, 2000.
3. S.G. Benjamin, K. J. Brundage, P. A. Miller, T. L. Smith, G. A. Grell, D. Kim, J. M. Brown, T. W. Schlatter, and L. L. Morone. The Rapid Update Cycle at NMC. In *Proc. Tenth Conference on Numerical Weather Prediction*, pages 566–568, Portland, OR, Jul. 1994.
4. A. Chutinan and B.H. Krogh. Verification of infinite-state dynamic systems using approximate quotient transition systems. *IEEE Transactions on Automatic Control*, 46(9):1401–1410, 2001.
5. R.E. Cole, C. Richard, S. Kim, and D. Bailey. An assessment of the 60 km rapid update cycle (RUC) with near real-time aircraft reports. Technical Report NASA/A-1, MIT Lincoln Laboratory, Jul. 1998.
6. R. Durrett. *Stochastic calculus: A practical introduction*. CRC Press, 1996.
7. H. Erzberger, R.A. Paielli, D.R. Isaacson, and M.M. Eshow. Conflict detection and resolution in the presence of prediction error. In *Proc. of the 1st USA/Europe Air Traffic Management R & D Seminar*, Saclay, France, June 1997.
8. J. Hu, J. Lygeros, M. Prandini, and S. Sastry. Aircraft conflict prediction and resolution using Brownian Motion. In *Proc. of the 38<sup>th</sup> Conf. on Decision and Control*, Phoenix, AZ, December 1999.
9. J. Hu and M. Prandini. Aircraft conflict detection: a method for computing the probability of conflict based on Markov chain approximation. In *European Control Conf.*, Cambridge, UK, September 2003.
10. J. Hu, M. Prandini, and S. Sastry. Optimal coordinated maneuvers for three dimensional aircraft conflict resolution. *Journal of Guidance, Control and Dynamics*, 25(5):888–900, 2002.
11. J. Hu, M. Prandini, and S. Sastry. Aircraft conflict detection in presence of spatially correlated wind perturbations. In *AIAA Guidance, Navigation, and Control Conference and Exhibit*, Austin, USA, August 2003.
12. J. Hu, M. Prandini, and S. Sastry. Probabilistic safety analysis in three dimensional aircraft flight. In *Proc. of the 42<sup>nd</sup> Conf. on Decision and Control*, Maui, USA, December 2003.
13. J. Hu, M. Prandini, and S. Sastry. Optimal coordinated motions for multiple agents moving on a plane. *SIAM Journal on Control and Optimization*, 42(2):637–668, 2003.
14. J. Hu, M. Prandini, and S. Sastry. Aircraft conflict prediction in presence of a spatially correlated wind field. *IEEE Transactions on Intelligent Transportation Systems*, 6(3):326–340, 2005.
15. E. H. Isaaks and R.M. Srivastava. *An Introduction to Applied Geostatistics*. Oxford University Press, 1989.
16. J. Kosecka, C. Tomlin, G.J. Pappas, and S. Sastry. Generation of Conflict Resolution Maneuvers For Air Traffic Management. In *Proc. of the IEEE Conference on Intelligent Robotics and System '97*, volume 3, pages 1598–1603, Grenoble, France, September 1997.
17. J. Krozel and M. Peters. Strategic conflict detection and resolution for free flight. In *Proc. of the 36<sup>th</sup> Conf. on Decision and Control*, volume 2, pages 1822–1828, San Diego, CA, December 1997.

18. J.K. Kuchar and L.C. Yang. A review of conflict detection and resolution modeling methods. *IEEE Transactions on Intelligent Transportation Systems, Special Issue on Air Traffic Control - Part I*, 1(4):179–189, 2000.
19. A.B. Kurzhanski and P. Varaiya. Ellipsoidal techniques for reachability analysis. In B. Krogh and N. Lynch, editors, *Hybrid Systems: Computation and Control*, Lecture Notes in Computer Science, pages 202–214. Springer Verlag, 2000.
20. A.B. Kurzhanski and P. Varaiya. On reachability under uncertainty. *SIAM J. Control Optim.*, 41(1):181–216, 2002.
21. J. Lygeros and N. Lynch. On the formal verification of the TCAS conflict resolution algorithms. In *Proc. of the 36<sup>th</sup> Conf. on Decision and Control*, pages 1829–1834, San Diego, CA, December 1997.
22. J. Lygeros and M. Prandini. Aircraft and weather models for probabilistic conflict detection. In *Proc. of the 41<sup>st</sup> Conf. on Decision and Control*, Las Vegas, NV, December 2002.
23. F. Medioni, N. Durand, and J.M. Alliot. Air traffic conflict resolution by genetic algorithms. In *Proc. of the Artificial Evolution, European Conference (AE 95)*, pages 370–383, Brest, France, September 1995.
24. P.K. Menon, G.D. Sweriduk, and B. Sridhar. Optimal strategies for free-flight air traffic conflict resolution. *Journal of Guidance, Control, and Dynamics*, 22(2):202–211, 1999.
25. I. Mitchell, A. Bayen, and C. Tomlin. Validating a Hamilton-Jacobi approximation to hybrid system reachable sets. In A. Sangiovanni-Vincentelli and M. Di Benedetto, editors, *Hybrid Systems: Computation and Control*, Lecture Notes in Computer Science, pages 418–432. Springer Verlag, 2001.
26. I. Mitchell and C. Tomlin. Level set methods for computation in hybrid systems. In B. Krogh and N. Lynch, editors, *Hybrid Systems: Computation and Control*, Lecture Notes in Computer Science, pages 310–323. Springer Verlag, 2000.
27. R.A. Paielli and H. Erzberger. Conflict probability estimation for free flight. *Journal of Guidance, Control, and Dynamics*, 20(3):588–596, 1997.
28. M. Prandini, J. Hu, J. Lygeros, and S. Sastry. A probabilistic approach to aircraft conflict detection. *IEEE Transactions on Intelligent Transportation Systems, Special Issue on Air Traffic Control - Part I*, 1(4):199–220, 2000.
29. Radio Technical Commission for Aeronautics. Minimum operational performance standards for traffic alert and collision avoidance system (TCAS) air-born equipment. Technical Report RTCA/DO-185, RTCA, September 1990. Consolidated Edition.
30. J. Schröder and J. Lunze. Representation of quantised systems by the Frobenius-Perron operator. In A. Sangiovanni-Vincentelli and M. Di Benedetto, editors, *Hybrid Systems: Computation and Control*, Lecture Notes in Computer Science, pages 473–486. Springer Verlag, 2001.
31. D.W. Stroock and S.R.S. Varadhan. *Multidimensional Diffusion Processes*. Springer-Verlag, 1979.
32. C. Tomlin, I. Mitchell, A. Bayen, and M. Oishi. Computational techniques for the verification and control of hybrid systems. *Proceedings of the IEEE*, 91(7):986–1001, 2003.
33. C. Tomlin, G.J. Pappas, and S. Sastry. Conflict resolution for air traffic management: A study in multi-agent hybrid systems. *IEEE Transactions on Automatic Control*, 43(4):509–521, 1998.

34. L.C. Yang and J. Kuchar. Prototype conflict alerting system for free flight. In *Proc. of the AIAA 35th Aerospace Sciences Meeting, AIAA-97-0220*, Reno, NV, January 1997.
35. Y. Zhao and R. Schultz. Deterministic resolution of two aircraft conflict in free flight. In *Proc. of the AIAA Guidance, Navigation, and Control Conference, AIAA-97-3547*, New Orleans, LA, August 1997.